This is the Pre-Published Version.
X. Huang & J. Gao (2020) *A Review of Near-limit Opposed Fire Spread*, **Fire Safety Journal** – Special Issue of IAFSS International Symposium. https://doi.org/10.1016/j.firesaf.2020.103141

A Review of Near-limit Opposed Fire Spread

Xinyan Huang [a,b,*], Jian Gao [c,*]

[a] *Department of Building Services Engineering, Hong Kong Polytechnic University, Hong Kong*

[b] *The Hong Kong Polytechnic University Shenzhen Research Institute, Shenzhen 518057, China*

[c] *Key Laboratory of Biofuels, Qingdao Institute of Bioenergy and Bioprocess Technology, Chinese Academy of Sciences, Qingdao 266101, China*

Corresponding author: xy.huang@polyu.edu.hk, gaojian@qibebt.ac.cn

Abstract: Creeping fire spread under opposed airflow is a classic fundamental fire research problem involving heat transfer, fluid dynamics, chemical kinetics, and is strongly dependent on environmental factors. Persistent research over the last 50 years has established a solid framework for different fire-spread processes, but new fire phenomena and recent developments continue to challenge our current understanding and inspire future research areas. In this review, we revisit the problem of opposed fire spread under limited and excessive oxygen supply. Various near-limit fire phenomena, as recently observed in flaming, smoldering, and glowing spread under various environment and fuel configurations, are reviewed in detail. Particularly, aspects of apparent importance, such as transition phenomena and heterogenous chemistry, in near-limit fire spread are highlighted, and valuable problems for future research are suggested.

***Keywords*:** Creeping flame spread; Extinction; Fingering spread; Glowing; Smoldering;

Nomenclature

Symbols		***Greeks***	
A	area (m^2)	α	Thermal diffusivity (m^2/s)
B	mass transfer number (-)	β	volumetric expansion coefficient (1/K)
c	specific heat (kJ/kg/K)	δ	solid-phase length (mm)
D	molecular diffusivity (m^2/s)	ρ	density (kg/m^3)
Da	Damkohler number (-)	λ	thermal conductivity (W/m-K)
Gr	Grashof number (-)	ν	kinematic viscosity (m^2/s)
h	convection coefficent (W/m^2-K)	φ	equivalence ratio (-)
Δh	enthalpy change (J/kg)	$\dot{\omega}$	reaction rate (1/s)
H	height (m)	***Superscripts***	
ΔH	heat of reaction (MJ/kg)	*	crtical
L	gas-phase length (m)		
LOC	limiting oxygen concentration	**Subscripts**	
Le	Lewis number (-)	0	initial
Nu	Nusselt number (-)	a	ambient or air
$\dot{m}$	mass-loss rate (kg/s)	b	burning or buoyancy
$\dot{m}''$	mass loss flux (kg/m^2-s)	ch	chemical
$MLOC$	minimum LOC	eff	effective
p	perimeter (m)	f	fire
P	pressure (Pa)	fl	flame
Pe	Peclet number (-)	F	fuel
$\dot{q}''$	heat flux (kW/m^2)	g	gas
$\dot{R}$	regression rate (m/s)	ig	ignition
StF	smoldering-to-flaming	$loss$	heat loss
StR	spread-to-regression	O_2	oxygen
t	time (s)	ox	oxidation
T	temperature (°C)	p	preheating
U	airflow speed (m/s)	py	pyrolysis
V_f	fire-spread rate (mm/s)	s	surface
X	volume fraction (%)	sr	surface reradiation
Y	mass fraction (%)	sm	smoldering

1. Introduction

Fire spread shows the relative motion between the fire front and fuel that plays a critical role in evaluating the risk and hazard of fire. Generally, the spread of fire is a result of continuous ignition through heat transfer (e.g. convection, conduction and radiation from the hot smoke, flame, and solid surface) or mass transfer (e.g. evaporation, pyrolysis, spotting, and dripping). More specifically, fire spread characterizes the motion of the boundary between unburnt and burning combustibles, communicated by combustion processes ranging from *vigorous flaming* and *visible glowing* to *hidden smoldering* [1].

The spread of flame is a surface phenomenon, which requires the flame to heat the fuel surface to its *ignition temperature*, roughly the pyrolysis point for solid and the flashpoint for liquid fuels; and then, released fuel gases need to mix with oxygen and pilot by the flame. Since the 1960s, flame spread has been a hot research topic in both combustion and fire communities and first reviewed by Emmons [2] and Friedman [3]. Williams [1] summarized fundamental mechanisms of chemistry and transport in different types of fire-spread processes and underpinned a group of analytical equations for determining the fire-spread rate and limiting conditions.

The difference between concurrent (forward) and opposed (reverse) fire spread, as well as their modeling methods were systematically discussed by Fernandez-Pello and Hirano [4–7]. A later review by Wichman [6] focused on the theory for the opposed flame spread, as well as its historical and logical development. Recently, concurrent flame spread was reviewed by Gollner *et al.* [8] with an emphasis on the effect of flow and geometry. Fire spread over liquid fuels was reviewed by Ross [9]; and Ohlemiller [10] reviewed smoldering spread. Along with these classic reviews, more research have explored fire spread for different fuel types (discrete and composite) and fire scenarios (e.g. wildland fire and façade fire), as well as, the influence of environmental parameters (e.g. wind, pressure, and microgravity), so that our understanding of fire spread continues to grow.

Phenomenologically, the rate of fire spread (V_f) is equivalent to the speed of ignition or the expansion speed of the burning region as

$$V_f = \frac{\Delta x}{t_{ig}} = \frac{dA_b}{pdt} \tag{1}$$

where t_{ig} is the ignition time for the fuel that is Δx away from the fire inception, p is the perimeter of the burning area (A_b). Physically, the fire spread rate is controlled by the ratio between heat transfer in fire (driving force) and fuel thermal inertia (resistance) [1,2] as

$$V_f = \frac{\dot{q}_f''}{\rho_F \Delta h_F} = \frac{\dot{q}_f'' L_p}{\rho_F \delta_T c_F \left(T_{ig} - T_0\right)} = \frac{\text{Fire scenario}}{\text{Material properties}} \tag{2}$$

where ρ is the surface fuel density, Δh is the difference in thermal enthalpy per unit mass between the virgin fuel and its ignition temperature (T_{ig} or the minimum gasification temperature), and δ_T is the thermal depth of fuel. The effective heat flux of the fire ($\dot{q}_f''$) with the reduction of heat loss and the preheating length (L_p) are related to the power of fire, but more importantly, the heat transfer efficiency from the burning region to the unburnt fuel.

Note that Eq. (2) only provides a qualitative description, because of 1) unknown material properties, 2) simplified heat-transfer process and ignition temperature from complex solid-phase reactions, and 3) ignoring the gas-phase chemistry. Today, a quantitative and numerical solution of V_f, resolving detailed gas- and solid-phase chemistry and heat-transfer process, is still challenging. Even for a "simple" problem of flame spread over well-known fuel, such as polymethyl methacrylate (PMMA), it is still difficult to calculate and predict the flame-spread rate without tuning some unknown parameters.

Depending on the direction of airflow (or wind) and fire spread, concurrent fire spread and opposed fire spread modes can be distinguished, as illustrated in Fig. 1. Given the fire-induced upward buoyancy flow, upward/downward fire spread is the most common mode of concurrent/opposed fire spread. In the wildland fire communities, heading/backing fire is often used for concurrent/opposed fire spread [11]. Before discussing the near-limit conditions of the opposed fire spread, the similarities and differences of opposed and concurrent fire spread are briefly introduced for both flaming and smoldering (Section 1.1 and 1.2).

1.1. Concurrent vs. Opposed Flame Spread

To sustain a flame on solid fuel, both heterogenous pyrolysis reactions and homogenous flaming reactions are required, and these global reactions can be expressed as

$$\text{Fuel (s)} \xrightarrow{\text{Heat}} \text{Pyrolyzate (g)} + \text{Char (s)} \qquad \text{[Pyrolysis]} \tag{3a}$$

$$\text{Pyrolyzate (g)} + \text{O}_2 \rightarrow \text{Gases} \qquad \text{[Flaming]} \tag{3b}$$

For flame spread, the thermal depth of fuel (δ_T) depends on the fuel thickness (δ_F) and the flame heating rate. Therefore, the flame-spread rate for thick and thin fuels [12] may be approximated as

$$V_{fl} = \begin{cases} \dfrac{\dot{q}''_{fl} L_p}{\rho_F \delta_F c_F (T_{ig} - T_0)} & \text{(thin fuel, } \delta_T = \delta_F\text{)} \\ \dfrac{\dot{q}''^{\,2}_{fl} L_p}{\rho_F \lambda_F c_F (T_{ig} - T_0)^2} & \text{(thick fuel, } \delta_T = \dfrac{\lambda_F (T_{ig} - T_0)}{\dot{q}''_{fl}} \approx \sqrt{\dfrac{\alpha_F L_f}{V_{fl}}}\text{)} \end{cases} \tag{4}$$

The equation ignores the conductive heat transfer in the solid phase that has a crucial role in near-limit spread.

Figure 1(a) illustrates an example of opposed and concurrent flame spread over a thick charring solid fuel, such as a wood plate. Both concurrent and opposed flame spread exist, because the flame is always spreading from the burning fuel to unburnt fuels that are available at both upstream and downstream. Nevertheless, even if flame spreads in both directions, the concurrent flame spread generally dominates the fire development, such as the upward flame spread over the building façade and upslope spreading of a wildfire [8]. It is because the opposed flame spread is much slower, whereas the concurrent flame spread increases significantly with the wind speed (Fig. 2a), due to the increase in the preheating length (L_p) and heat flux ($\dot{q}''_{fl}$) of flame [5,11,13–15]. It is also relatively easier to blow off the flame in the opposed flow. If local burnout occurs, two independent flames, spreading towards unburned fuel upstream and downstream, can be observed.

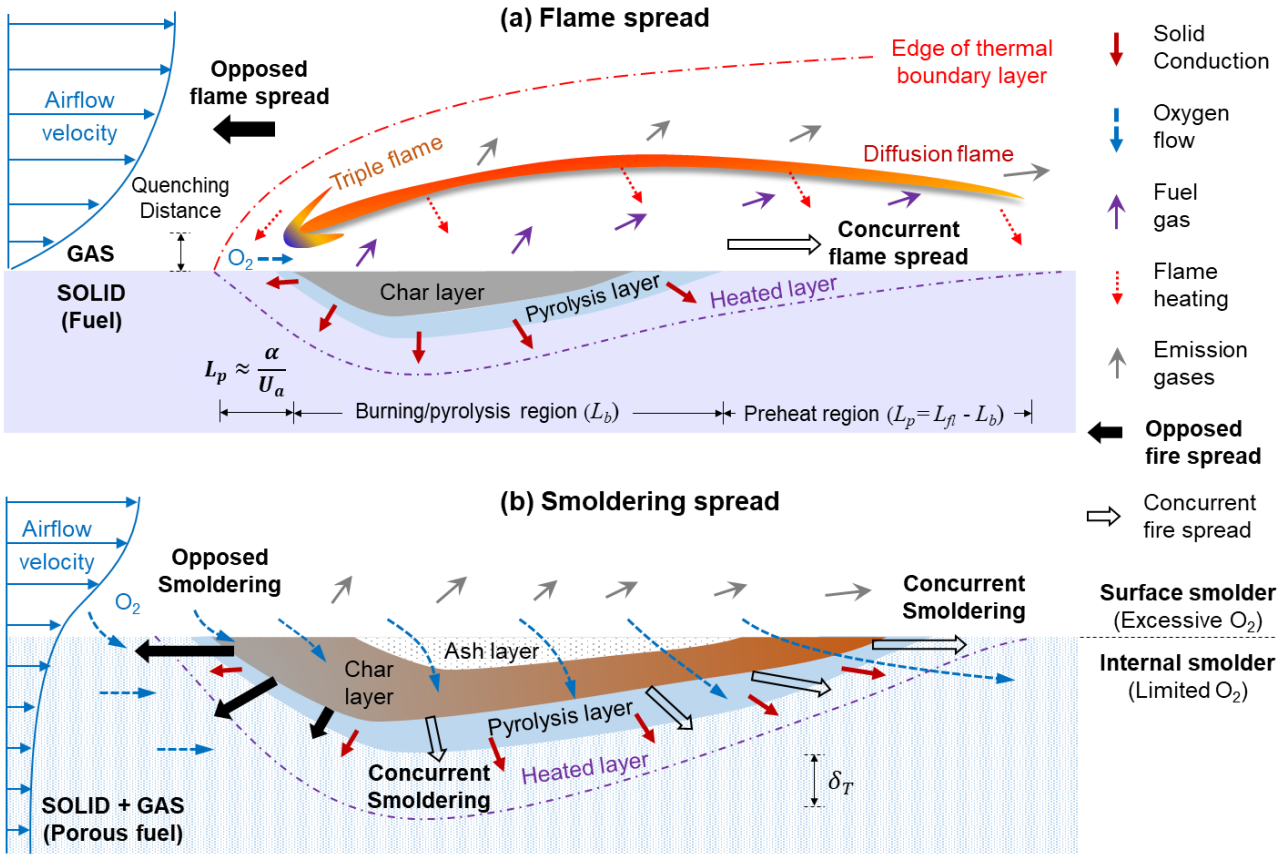

Fig. 1. Diagrams of the concurrent (forward) vs. opposed (reverse) fire spread, (a) flame, and (b) smoldering.

The opposed flame spread is also called upstream flame spread or creeping flame spread because of a much smaller spread rate [16–18]. Under flame-induced upward buoyant flow, the flame spreads horizontally over the flat fuel against the buoyant flow is also a typical opposed flame spread. For opposed flame spread, as the wind speed increases, the effective flame preheating length decreases, while the convective flame heat flux increases, satisfying

$$\rho U_a c_p (T_f - T_0) \approx \lambda_g (T_f - T_0)/L_p \Rightarrow L_p \approx \alpha_g / U_a \tag{5}$$

$$\dot{q}''_{fl} \approx h(T_f - T_0) \sim U_a \tag{6}$$

The preheating by the flame controls the flame spread at intermediate airflow velocities, namely, the "thermal-regime" behaviors [19,20]. Nevertheless, the thermal-regime airflow speed is generally less than the buoyant flow ($U_b \approx \sqrt{gh_f}$). Thus, the opposed flame spread on Earth is less sensitive to or slightly decreases with the wind speed, especially for thin solid fuels [19,21–23] and liquid fuels [9,24,25]. For the thick fuel, the thermal regime can be observed under a high oxygen concentration, because of the oxidative pyrolysis and non-negligible conductive preheating in the solid phase [4,26]. Further increasing the opposed flow, the opposed flame-spread rate falls gradually toward the blowoff limit because of the cooling effects on gas-phase reactions, namely, the Damkohler number (*Da*) effect [1,6] (Fig. 2a). For charring materials, the flame can be easily blown off, because the accumulated char layer restrains the flame from heating the fuel in-depth [27].

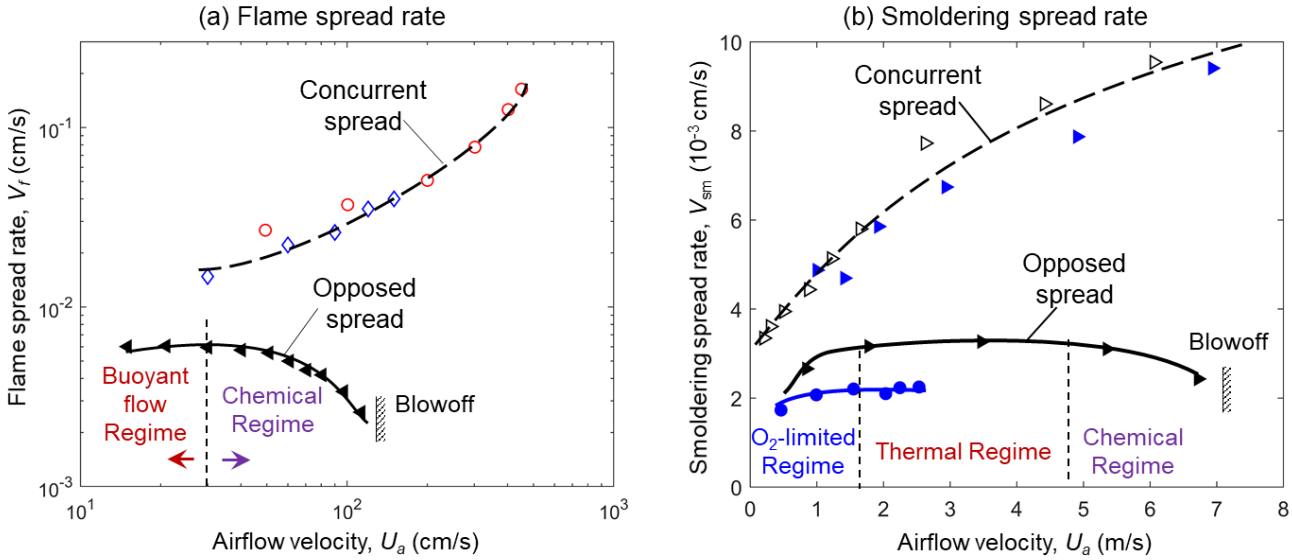

Fig. 2. Rate of the concurrent (forward) vs. opposed (reverse) fire spread, (a) flame spread over the thick PMMA plane (◀ [19] and ○ [5]) and wire (◊ [13]), and (b) surface smoldering spread over a beech sawdust layer (●) and several different fiberboards (▶,▷,▸) [28].

1.2. Concurrent vs. Opposed Smoldering Spread

Smoldering is the slow, low-temperature, flameless burning of porous fuels, and the most persistent combustion phenomenon [29]. Smoldering shares the same pyrolysis reactions (Eq. 3a) with flaming, but requires the production of char and heterogeneous (or surface) char oxidation [10,29]

$$\text{Char (s)} + O_2 \rightarrow \text{Gases} + \text{Ash (s)} \qquad \text{[Smoldering]} \tag{3c}$$

The threshold temperature of char oxidation ($T_{ig,sm}$ ≈250-300℃ [30–32]) is much lower than that of a flame (~1300 K) [33]. Thus, the relatively "cool" smoldering front can be sustained in temperatures as low as 250℃ near the quenching limit [32,34]. Because of the large thermal inertia ($\rho c \lambda$) of solid fuel and limited oxygen supply into the porous fuel bed, the smoldering temperature is typically below 700℃ but can be higher than 1000℃ for high-density fuel under a sufficient oxygen supply [35,36].

Figure 1(b) shows a typical opposed and concurrent smoldering spread over a porous solid fuel. Considering smoldering is a 3D volumetric phenomenon [29], "spread" that generally describes a surface

phenomenon may not be comprehensive, especially for the internal smoldering process below the free surface[#] [28,37–40]. Depending on the accessibility of oxygen to the original fuel, smoldering motion has two modes:

(I) *Surface smoldering spread* over the interface between fuel and ambient, where opposed spread is usually slower than concurrent spread [28] (Fig. 2b).

(II) *Internal smoldering spread* inside the porous fuel, where opposed spread is usually faster than concurrent spread [32,39].

For internal smoldering in low-permeability consolidated fuels (e.g. wood and incense), only concurrent spread is possible because oxygen can only enter from the porous charred side. Thus, the concurrent smoldering "spread" is essentially a burning and fuel-regression process, similar to the burning of a candle or the premixed flame. The observed concurrent smoldering rate is the regression rate ($\dot{R}$) as

$$V_{sm} = \dot{R} = \frac{\dot{m}''_F}{\rho_F} = \frac{\dot{m}''_{O_2}}{\gamma_{O_2}\rho_F} = \frac{\rho_a Y_{O_2}}{\gamma_{O_2}\rho_F} U_a \tag{7}$$

where $\dot{m}''_F$ is the burning flux of fuel, $\dot{m}''_{O_2} = Y_{O_2}\rho_a U_a$ is the mass flux of oxygen, γ_{O_2} is the stoichiometric coefficient for oxygen. Therefore, the concurrent smoldering "spread" rate increases as the fuel density (ρ_F) decreases, or the airflow velocity (U_a) increases [28,41] (Fig. 2b). For most internal smoldering spread, the oxygen supply also controls the smoldering spread (Section 2.3).

Smoldering needs no pilot source, and all smoldering-ignition processes can be viewed as *to provide an environment that enables the self-ignition of fuel*. Therefore, smoldering spread may also be viewed as a continuous self-ignition process. For smoldering, the heating length equals the thermal depth of fuel ($L_f = \delta_T$) in Eq. (2). Thus, under a sufficient oxygen supply, the rate of opposed smoldering spread may be expressed as

$$V_{sm} = \frac{\dot{q}''_f}{\rho_F \Delta h_F} = \sqrt{\frac{\alpha_F \dot{\omega}_{ig} \Delta H_{sm}}{c_F\left(T_{ig,sm} - T_0\right)}} \approx \frac{\alpha_F}{\delta_T} \quad \text{(sufficient } O_2\text{)} \tag{8}$$

where $\dot{q}''_f = \lambda_F\left(T_{ig,sm} - T_0\right)/\delta_T \approx \rho_F \dot{\omega}_{ig} \Delta H_{sm} \delta_T$, α_F is the fuel thermal diffusivity, $\dot{\omega}_{ig} = Ze^{-E/RT_{ig,sm}}$ is a minimum fuel oxidation rate, and ΔH_{sm} is the heat of smoldering combustion. Therefore, opposed smoldering spread is mainly controlled by the fuel chemistry and conduction, while insensitive to the airflow velocity. Thus, it may also be called as the "Thermal Regime" like the flame spread, as compared between Fig. 2(a) and (b).

If the wind cooling effect exceeds its effect of enhanced oxygen supply, the surface spread of smoldering cannot be sustained, but changes to internal spread to minimize the heat loss and form a structure of overhang [38]. As the oxygen supply increases, the excessive oxygen can support further gas-phase homogenous oxidations, resulting in smoldering-to-flaming (StF) transition (Section 3.2) or glowing (Section 3.3). When the wind is extremely high, fuel particles maybe blown away (e.g. firebrand [42] or fluidized bed [41]), and the blowoff of smoldering is also possible [28] (Section 3.4).

1.3. Near-Limit Opposed Fire Spread Phenomena

Essentially, most near-extinction fire spread can be explained by some critical Damkohler number (Da^*), when the flow residence time scale (t_r) is close to the reaction time scale (t_{ch}) for blowoff as

$$Da^* = \frac{t_r}{t_{ch}} \sim O(1) \tag{9}$$

or when a system length scale is comparable to the size of reaction zone (quenching), as reviewed by Williams [1] and Wickman [6]. Notably, condensed-phase transport (e.g. conduction, surface re-radiation, drying, and phase change) and chemical reactions (e.g. pyrolysis, and heterogeneous oxidation) start to play vital roles in extinction. At the same time, effects of chemistry, radiation, and diffusion would be magnified near extinction limits. Figure 3 shows typical opposed fire-spread configurations with decreasing oxygen supply.

[#] Free surface in this paper is defined as the interface between ambient and the bulk fuel.

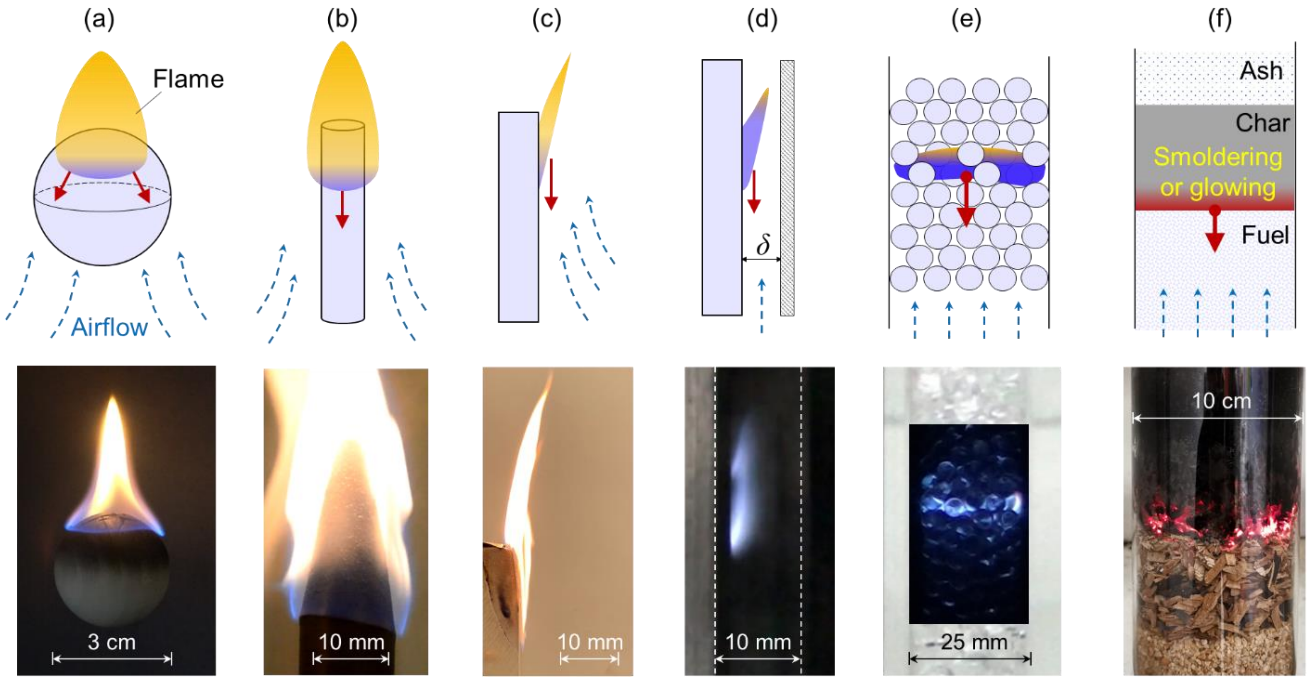

Fig. 3. Opposed fire spread with decreasing oxygen supply, (a) sphere wood fuel, (b) cylindrical rod [43], (c) flat plate, (d) narrow channel (credit: Feng Zhu), (e) particle bed with blue flame, (f) porous fuel bed with smoldering or glowing, where fuel in (b-e) is PMMA and in (a,f) is wood; red arrow shows the fire spread direction, and blue dashed arrow shows air supply.

Depending on the selected references (e.g. the normal ambient or a reference fuel), different factors could be *highlighted* for the same near-limit behavior. For example, for near-extinction flame spread over electrical wire under a low opposed flow [44], the smothering process is highlighted, if compared to the normal ambient. Alternatively, the cooling effect or quenching of the conductive wire core can be highlighted, if compared to a simple fuel. These different dominant factors for near-limit behaviors will be carefully identified along with the discussion in the following sections.

As opposed fire-spread theories have been summarized in great detail [1,6], this review is devoted to various near-limit transition and extinction phenomena that are recently observed in flaming and smoldering spread. As the concept of opposed fire spread is bound to the interaction between opposed airflow and fuel, fire spread over different fuel configurations (Fig. 3) under limited and excessive airflow will be focused on. Finally, unsolved challenges are summarized, and related future research opportunities will be discussed.

2. Opposed Fire Spread in Limited Oxygen

In terms of fire spread, “oxygen-limited” may have three meanings, (1) the absence of buoyancy-induced oxygen supply, (2) small airflow velocity, or (3) low oxygen concentration (X_{O_2}). Under limited oxygen supply, opposed fire spread prevails because its fire inception is closer to the fresh air upstream. In contrast, concurrent fire spread, which tends to expand the burning area and increase fuel production, becomes unstable, where the downstream fire inception either exceeds the rich flammability limit or receives no oxygen to maintain smoldering. Consequently, the initial bi-directional fire spread after ignition (Fig. 1) can no longer be sustained, and only the opposed fire spread survives [45–48].

On the other hand, as the ambient oxygen concentration decreases, extinction eventually occurs, leading to the concept of limiting oxygen concentration (LOC). Compared to concurrent flame spread, opposed flame spread has a higher LOC [4,49,50], because a much smaller portion of flame heat release is transferred to the upstream preheating region, as compared in Fig. 1(a). This section reviews several opposed fire-spread behaviors under oxygen-limited conditions (or near smothering), including microgravity, fingering, and internal smoldering.

2.1. Limited buoyant flow and microgravity

In normal-gravity (1g) on Earth, the fire-induced buoyant flow creates a positive feedback between oxygen supply and fire to promote the fire growth. In contrast, in absence of buoyancy-induced convective flow, microgravity (μg) is naturally an oxygen-limited environment for fire spread [51]. The near-limit fire spread and material flammability in microgravity (Fig. 4a-c) are most relevant to the fire safety of manned spacecraft, where oxygen and ventilation systems are available to support both human activities and fire [52–54]. As high-cost microgravity tests and data are limited, ground experiments under low-pressure [55] or narrow-channel [56] are also widely used to simulate microgravity environment by reducing Grashof number (*Gr*),

$$Gr = \frac{\text{Buoyancy momentum}}{\text{Diffusion momentum}} = \frac{\rho^2 \beta g \Delta T H^3}{\mu^2} \propto gP^2H^3 \tag{10}$$

where reducing pressure lowers the buoyancy momentum. For instance, reducing the length scale (*H*) or pressure (*P*) to 1/10 will achieve the same *Gr* under 10^{-3} g or 10^{-2} g. Fundamentally, decreasing the pressure reduces the momentum of buoyant flow, whereas the dynamic viscosity (μ) is unaffected. Note that with a flame, the flame height (H_f) and temperature can also change with pressure.

Under the low-flow microgravity environment, the flame is prone to spread against the airflow after ignition [45–48] or form a finger spread (Section 2.3), in order to reach out for more oxygen. Kashiwagi *et al.* [45,57] first noticed the preference of opposed flame spread under microgravity after igniting a thin paper in the center (Fig. 4a), and similar behavior was also found for thick PMMA rods [47]. Olson *et al.* [46] found that concurrent flame spread was only possible after the burnout of fuel in the opposed flame spread. Recently, Vetturini *et al.* [48] found that when the flame spread rate over ultra-thin fuel was faster than concurrent airflow speed, it transitioned to a slower opposed flame spread mode that produced gaseous fuel at a lower rate (Fig. 4c). It is worth exploring the minimum airflow rate in microgravity and the minimum gravity level that allows bi-directional flame spread through future space and ground experiments.

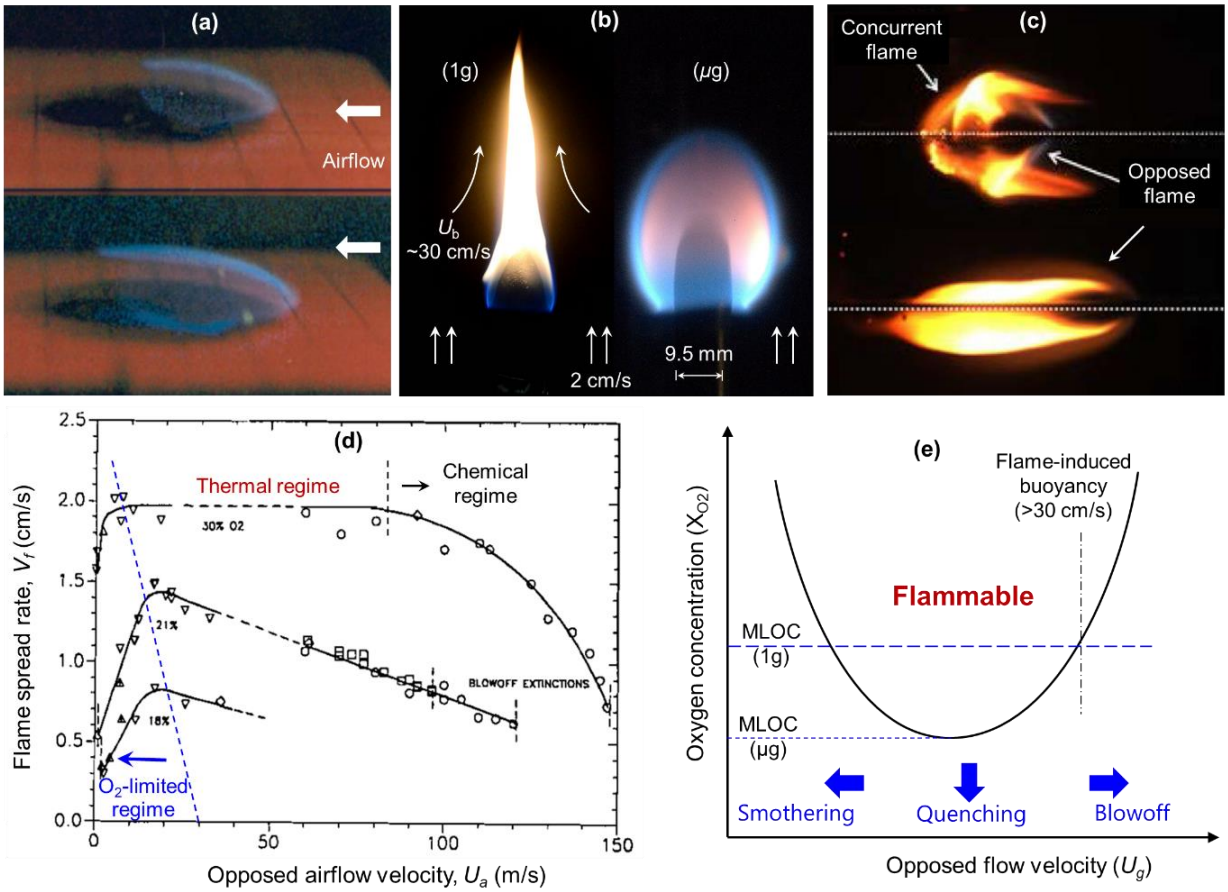

Fig. 4. Opposed flame spread in microgravity (a) after central ignition of paper [45], (b) over PMMA rod [47], (c) transition from concurrent to opposed flame spread [48], (d) flame-spread rate over thin paper under low-speed opposed flow [58], and (e) microgravity flammability map and extinction region [58,59].

As the μg airflow velocity further decreases, it enters the "Oxygen-Limited Regime," where flame becomes weak and moves away from the solid surface to seek for more oxygen, i.e., a thicker boundary layer, so that the heat transfer from the flame to fuel surface is decreased to slow down the flame spread. For the thin cellulose sheet, Olson [58] observed such oxygen-limited behavior at U_a < 15 cm/s for X_{O_2} = 30% and U_a < 25 cm/s for X_{O_2} = 21% (Fig. 4d). For thick fuels, such an oxygen-limited regime merges with the thermal regime [60], so its exact boundary is unclear. Different from blowoff, extinction that occurs under low flow velocity [61] is simply because the flame cannot survive without a sufficient oxygen supply, i.e., *smothering*. Therefore, in the quiescent microgravity ambient (U_a = 0), the flame generally cannot be sustained [49], unless the flame spread is fast enough to create a large relative velocity to ambient [48], or the flame heat transfer is enhanced in the high oxygen level or around a high-curvature fuel. Like microgravity droplet combustion, the flame can be sustained, if the solid fuel diameter is small enough [62] and tends to spread along the edges of fuel [63].

From the viewpoint of heat transfer, both the surface re-radiation and flame radiation heat loss become critical in oxygen-limited extinction:

(1) As the flame becomes weak, eventually, the flame heating cannot balance the re-radiation heat loss from the solid fuel surface which has to be maintained above the pyrolysis point (> 300°C) [64].

(2) As the airflow velocity decreases, the rapid decrease of heat release rate in the flame sheet cannot balance the slower decrease of flame radiation heat loss, similar to the extinction observed for low-stretch-rate counterflow diffusion flames [65,66].

Hence, researchers used "radiation extinction" [67,68] or "quenching" [58,69] to highlight the role of radiation heat loss (Fig. 4e), but it is still unclear whether the surface re-radiation or the flame radiation heat loss first triggers the extinction. For a thick fuel, the solid-phase conduction heat loss should also not be overlooked [53,70], and a deeper understanding may be achieved by microgravity flame-spread experiments under controlled external radiant heat fluxes.

On the other hand, the microgravity environment can prevent the buoyancy-induced blowoff, thus, extending the flammability to a lower oxygen concentration (Fig. 4e) [53,58]. The recent review by Fujita [53] summarized the latest understanding of the gravity influence on the material flammability limit. A lower LOC has been observed in microgravity and reduced gravity [44,60,71]. For example, the LOC decreases from 19% (1g) to 16% (ug) for a thin copper-core wire [44] and from 18% (1g) to 16.5% (ug) for a thick PMMA rod [60]. Moreover, if the airflow velocity is small, opposed flame spread can be even faster than concurrent flame spread, as observed in microgravity [46,72] and the narrow-channel experiment [50]. Nevertheless, the influence of ignition and development of the flow boundary layer may no longer be ignored for near-limit fire spread [22,73].

2.2. Fingering Spread

Under oxygen-limited conditions, fire spread over a solid fuel can break up into separated combustion fronts without consuming all the fuel, namely, the fingering-spread phenomenon. Fingering fire spread is persistent and able to extend the flammability of solid fuels; thus, it has been a hot research topic in the past three decades. Figure 5(a-f) show several typical fingering spread examples on thin [74–78] and thick fuel plates [79,80] and particle fuel bed [81] in forms of gas-fuel flames [82,83], flaming [74,79], smoldering and glowing [75–78,81]; in microgravity [78] and normal-gravity narrow channels [74–77,79,81–83]; as well as under both opposed and concurrent airflows [84,85].

Previous studies suggested two requirements for the occurrence of fingering spread,

(1) the limited oxygen transport to and/or intense heat loss from the combustion front that initiates local extinction and separated fire-spread fronts; and

(2) a small hybrid solid-phase/gas-phase Lewis number (*Le*), which enables the separated fire front to be self-sustained with a relatively large specific surface-to-volume ratio.

Separated flamelets over solid fuels were first observed by Zhang *et al*. [74] in 1992, by employing thin filter papers as the fuel samples that are vertically located in a closed chamber filled with several different groups of oxidant mixtures. They also changed the oxygen concentration and paper thickness to approach oxygen-limited extinction (or smothering) and used different diluents to vary the molecular diffusivity (*D*) and *Le* of

oxygen. Self-sustained separated flamelets (Fig. 5a), namely, the "cellular flame front" or under-developed fingering spread, were observed with *Le* = 0.31 (O_2/SF_6) and 0.56 (O_2/CO_2) near extinction limit.

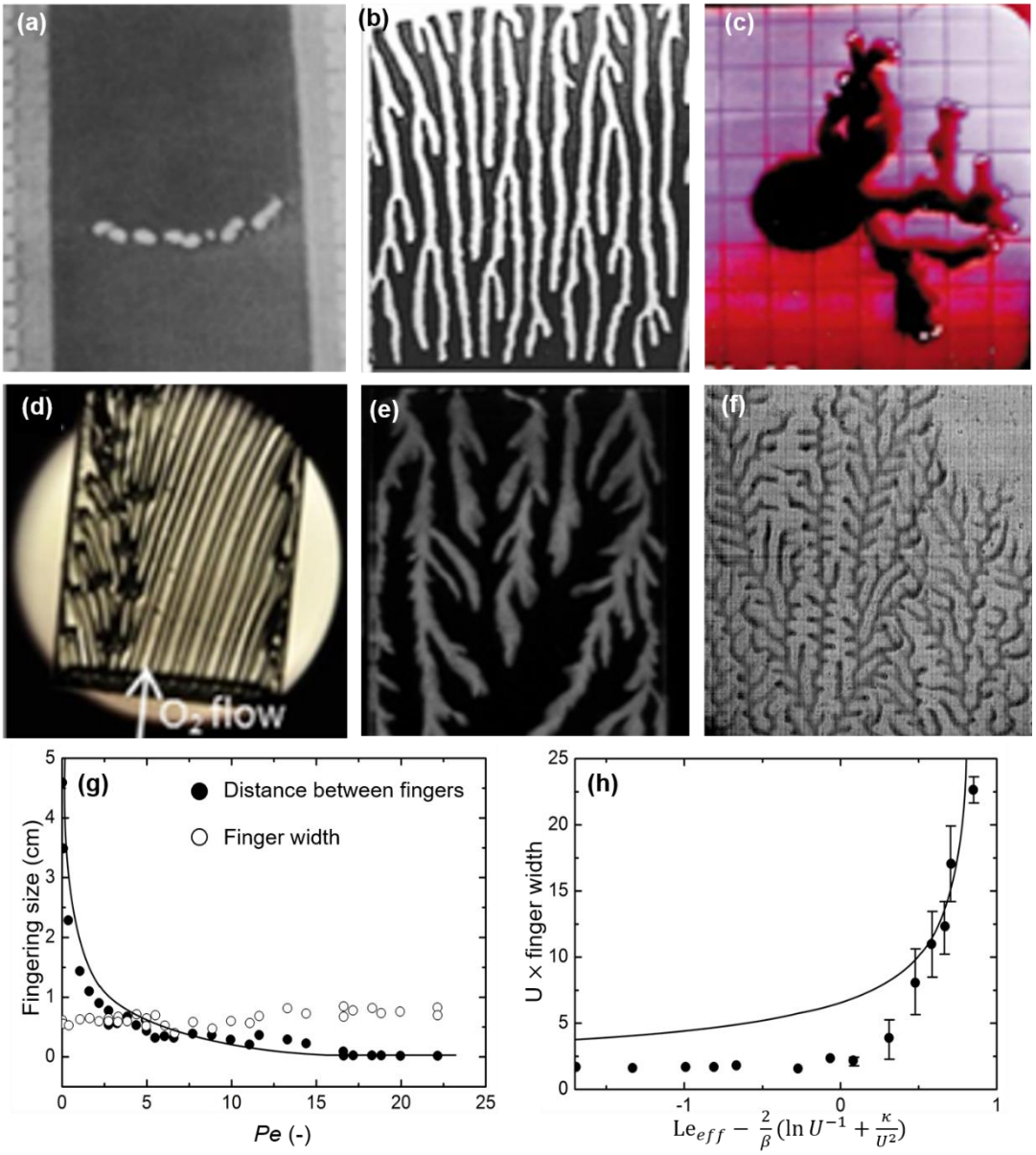

Fig. 5. Fingering spread, (a) flamelets (cellular flame) over thin filter paper [74]; (b) thin horizontal filter paper in a narrow gap [75–77]; (c) thin filter paper in microgravity [78]; (d) thick PMMA plate with flame [79]; (e) a bed of nano-aluminum particles [81]; (f) ultra-lean hydrogen flames in narrow Gaps; (g) fingering size as a function of *Pe* [75], and (h) finger width as a function of modified *Le* [86].

Later, Olson *et al.* [56,78,84] found that fingering smoldering fronts occurred in oxygen-limited microgravity by decreasing the flow speed (U_a), and suggested oxygen transport to be the onset factor for fingering spread. Zik *et al.* [75–77] found a similar fingering spread over thin papers in narrow-channel experiments. They determined the critical condition for fingering spread by the Peclet number (*Pe*)

$$Pe = \frac{U_a \delta}{D} \tag{11}$$

where the channel gap size (δ) needs to be sufficiently small to suppress vertical buoyant flow. A small *Pe* indicates that the oxygen diffusion velocity becomes comparable to the forced convective flow velocity. The value of *Pe* can quantify the distance between fingers, but not the fingering-spread rate and finger width (Fig. 5g). Thus, other numbers are needed to further determine fingering spread and the influence of fuel and environment.

To improve the prediction, several follow-up theoretical and numerical studies were performed to clarify the fingering-spread dynamics. Particularly, simplified 2D and 3D models that assume solid-gas thermal equilibrium [87–93] were developed to reproduce fingering fire spread. Such an equilibrium assumption requires defining an effective thermal diffusivity (α_{eff}) in order to simplify the two-phase combustion system,

$$\alpha_{\text{eff}} = \frac{\lambda_g(H-\delta_F)+\lambda_F\delta_F}{\rho_g c_{p,g}(H-\delta_F)+\ \rho_F c_{p,F}\delta_F} \tag{12}$$

where H is the height of the gap in which a combustible solid fuel plate burns, and δ_F is the thickness of the thin fuel [90] or the thermal depth for the thick fuel ($\delta_F = \delta_T$) [79]. Therefore, an effective Lewis number (Le_{eff}) may be defined as

$$Le_{\text{eff}} = \frac{\alpha_{\text{eff}}}{D_{O_2}} \tag{13}$$

where D_{O_2} is the diffusivity of oxygen. These numerical studies quantified that fingering spread could only appear when $Le_{\text{eff}} < 1$. Recent studies by Kuwana *et al.* [91] and Fuanshima *et al.* [92] further demonstrated that as long as the Le_{eff}, heat loss, and fuel properties were properly considered in the model, the fingering pattern and the spread rate could be quantitatively reproduced. For example, the finger width can be predicted by an equation combining effects of Le_{eff}, heat loss, and flow velocity (Fig. 5h).

Fingering fire spread over solid fuels is primarily driven by the imbalance between thermal and mass diffusive transports at oxygen-limited conditions. Therefore, it can be considered as *the analogy to the cellular flame* for premixed gas-phase combustion [33]. However, unlike the *Le* criteria for the cellular flame, α_{eff} and Le_{eff} are system properties rather than material properties. They are introduced with the assumption of solid-gas thermal equilibrium; thus, their validity and limitation require more explorations. For instance, the concept of Le_{eff} still cannot explain the influence of microgravity and oxygen concentration [56,78,84], because in microgravity with $h \gg \delta_F$, $Le_{\text{eff,}\mu g}$ in Eq. (13) becomes the conventional gas-phase *Le*. The latest 3D numerical work by Kumar *et al.* [94] also revealed that the fuel gas diffusivity could significantly influence the flamelet size, but it could not be explained by Le_{eff} if only oxygen diffusion is considered.

Moreover, coupled solid-gas properties and interaction between hetero- and homogeneous reactions may result in more complexities for fingering spread. For example, both smoldering and flaming fingering-spread modes have been observed [56], but limiting conditions for the transition between two spread modes have not been fully addressed. Between concurrent and opposed fingering spread, the differences regarding the initiation criteria, LOC, and spread patterns need more future research. Also, the influence of fuel geometry and surface boundary conditions on fingering spread has not been explored. Therefore, despite extensive experimental and numerical studies so far, ambiguities and mysteries still exist and warrant further efforts; thus, further study on fingering spread is of significance.

2.3. Smoldering spread inside Porous Media

As briefly mentioned in Section 1.2, smoldering spread inside porous media or internal smoldering is considered as the most oxygen-saving fire-spread mode (Fig. 3f), evident by the incomplete oxidation and a large amount of CO emissions [29,95]. For charring fuels, if the flame is smothered, smoldering could still survive. When the oxygen supply is limited, the internal smoldering spread rate is controlled by both the oxygen supply ($\dot{m}''_{O_2}$) and heat losses within the porous media ($\dot{q}''_{loss}$) [96,97], which is different from Eq. (8)

$$V_{sm} = \frac{\dot{q}''_f}{\rho_F \Delta h_F} \approx \frac{\dot{m}''_{O_2}\Delta H_{ox} - \dot{q}''_{loss}}{\rho_F c_F\left(T_{ig,sm} - T_0\right)} = \frac{\rho_a X_{O_2} U_a \Delta H_{ox} - \dot{q}''_{loss}}{\rho_F c_F\left(T_{ig,sm} - T_0\right)} \quad \text{(limited } O_2\text{)} \tag{14}$$

Thus, the opposed smoldering spread rate increases with the flow velocity. This "O_2-Limited" smoldering regime in Fig. 2(b) is similar to the opposed flame spread in Fig. 4(d) [28,98], which will be explored in this section.

Inside the porous fuel bed, smoldering tends to spread towards the free surface and opposed to the oxygen diffusion flow. The overall oxygen supply ($\dot{m}_{O_2}$) reduces with the increasing distance between the smoldering front and free surface (H) and the decreasing free-surface area (A_s) as

$$\dot{m}_{O_2} = \dot{m}''_{O_2} A_s = \rho_a X_{O_2} U_a A_s \sim \frac{A_s}{H} \tag{15}$$

where the airflow velocity ($U_a \propto H^{-1}$) follows the Darcy's law [99]. Palmer [28] studied upward smoldering spread over a heap of cork dust (Fig. 6a) where oxygen could diffuse to the reaction zone from both the top and side free surfaces. Smoldering could spread out from a depth of 90 cm, and the opposed spread rate increased as it approached the free surface (Fig. 6b). A similar upward (opposed) smoldering spread was found in peat fires, which was also faster than the downward (concurrent) spread [39].

On the other hand, the smoldering process involved in self-ignition is also a typical opposed spread. It is well known that the propensity of self-ignition increases with the bulk volume of porous fuel, and even if the depth of internal ignition spot increases, smoldering can still spread out [100]. It is because when the fuel volume increases, the increase in the free-surface area (A_s) is faster than the depth (H) in Eq. (15). Therefore, it is worth exploring both the maximum depth and the minimum free-surface area for maintaining internal smoldering spread.

Reducing the ambient pressure and gravity level also lowers the oxygen supply to smoldering [101]. There are very limited number of studies on smoldering spread under reduced pressure [35,102–104] (Fig. 6c). The observed smoldering extinction pressure of 10~20 kPa at X_{O_2} = 21% was higher than the observed 4 kPa for flame spread over thin paper [105], probably because smoldering could not enhance the buoyant oxygen supply as much as flaming. In recent microgravity Saffire experiments [106], an intense smoldering front was observed behind the weak flame front (Fig. 6d), suggesting that the influence of gravity on smoldering is much smaller than flaming. So far, except for fingering smolder spread over some thin fuels [56,78,84], microgravity data and numerical simulation on the minimum flowrate and LOC of smoldering spread are limited, so there is a big knowledge gap.

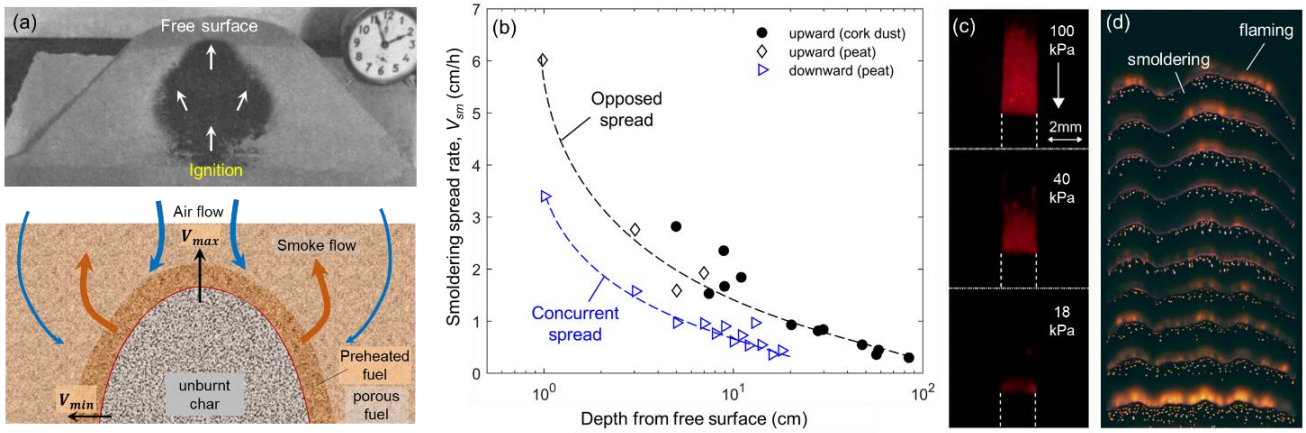

Fig. 6. (a) Upward smoldering spread inside cork dust towards the free surface [29] and schematic diagram [39], (b) opposed and concurrent smoldering spread rate the inside porous fuel [39], (c) pressure effect on opposed surface smoldering over incense [104], and (d) smoldering front behind the flaming front in microgravity [106].

By reducing the oxygen concentration, we can also define and measure the LOC of smoldering. Compared to flaming, the LOC for persistent smoldering is found to be much lower. For example, the LOC for smoldering peat fire is 15% [107], which increases with the fuel moisture [108,109]. Wang *et al.* [110] found LOC = 10% for the self-sustained opposed smoldering spread over pine chips, which can be further reduced to 6% with an external radiation. For self-ignition, Schmidt *et al.* [111] found that the smoldering fire could spread to the free surface under $X_{O_2} = 6\%$. Malow *et al.* [112] showed that lowering X_{O_2} to 5% could still not extinguish the smoldering fire on coal and wood chips.

The physical meaning for these small LOCs of smoldering in different experiments is still poorly understood. For a diffusion flame on solid or liquid fuel, LOC is mainly determined by the ease of phase change and mass transfer (i.e., the B number). A robust flame is required, but only a small portion of flame heat release is transferred to the burning region (Fig. 1a). In contrast, the oxygen supply and heat release of smoldering (Eqs. 14 and 15) can be equally increased by any of ρ_a (or P), X_{O_2}, U_a, and A_s. As most of the

reaction heat is directly conducted to the pyrolysis front, we can define LOC_{sm} when the spread is suspended or $V_{sm} = 0$ in Eq. (14)

$$LOC_{sm} \approx \frac{\dot{q}_{loss}}{\rho_g U_g A_s \Delta H_{ox}} \tag{16}$$

which depends on both the air supply and heat loss through fuel bed. If a $MLOC_{sm}$ has to be defined, it could be the minimum X_{O_2} to maintain the exothermic reaction ($\Delta H_{sm} > 0$), which can be measured from TGA-DSC tests.

3. Opposed Fire Spread in Excessive Oxygen

As the airflow (wind) velocity increases, opposed fire spread moves to the chemical regime, where the excessive air starts to cool the combustion front, and Da becomes small, so that the finite-rate combustion chemistry has to be considered. For the bi-directional flame spread in Fig. 1(a), a large wind destabilizes the opposed flame spread and only enables the concurrent flame spread, where the trailing-edge wake flame only causes the regression of local fuel (Section 3.1). Under excessive oxygen supply, the smoldering fire may transit to a flaming fire (Section 3.2) or co-exist with the flame to form a glowing spread (Section 3.3). A further increase of the flow velocity would eventually lead to blowoff (Section 3.4).

3.1. Spread-to-Regression (StR) Transition

Fire spread is always accompanied by burning and regression of fuel, but burning will not always result in a fire spread [1]. Typical burning and regression processes include the candle flame (Fig. 7a), liquid pool fire, and rocket propellant [113,114]. Because the regression of fuel surface also causes the movement of a fire, it is often confused with the fire spread (e.g. the concurrent smoldering and Eq. 7). Before blowoff, the spread of the flame will first stop and transition to fuel regression, so this section will review the spread-to-regression (StR) transition.

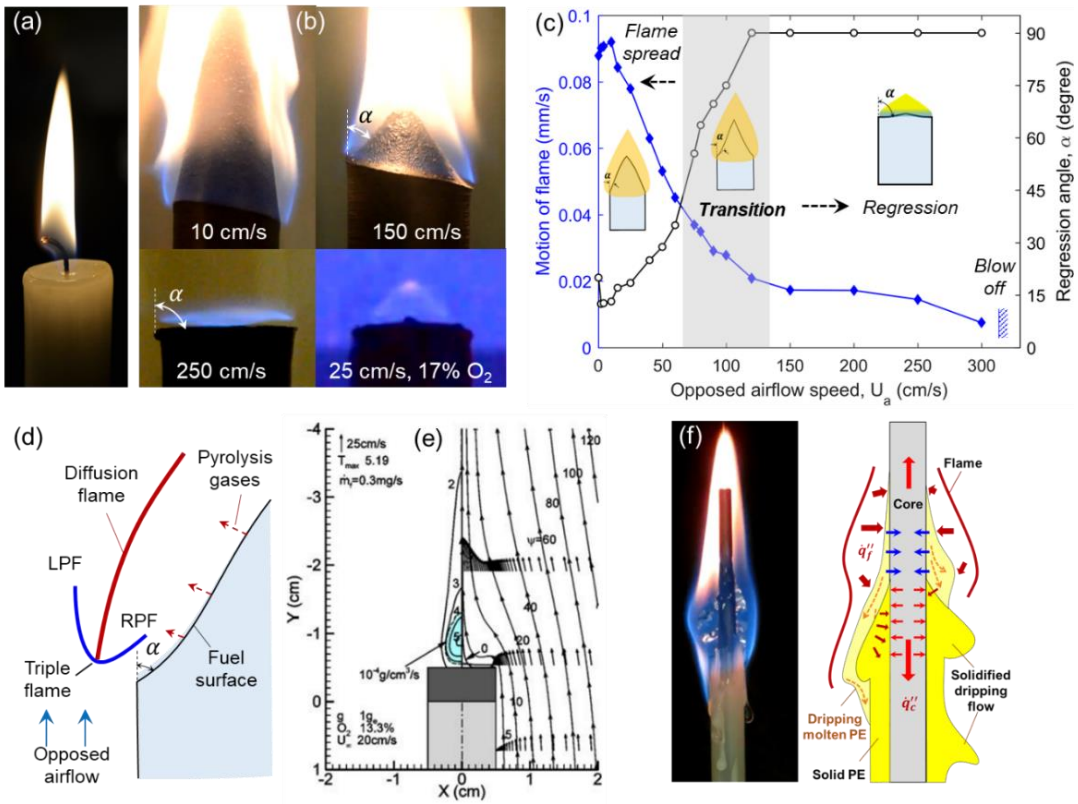

Fig. 7. (a) Burning and regression of a candle, (b) flame spread-to-regression (StR) transition on PMMA rods, (c) StR transition regimes varying with the opposed flow velocity, (d) the triple-flame structure and regression angle (α) [43], (e) numerical simulation of the wake flame and fuel regression [116], and (f) flame motion driven by dripping flow [23,121].

Under excessive airflow (Chemical Regime), flame spread slows down as the opposed flow increases. Both rates of flame spread and burning will reach steady-state, and the fuel regression angle (α) at the flame inception increases with the opposed flow (Fig. 7b-c). Eventually, the flame hides in the wake region like a candle flame and even forms a flat blue flame sheet above the fuel sample [43,115]. Because of a triple-flame structure in the flame leading edge (Fig. 7d), *flame spread transitions to fuel regression when the opposed flow velocity is larger than the local laminar burning velocity* (about 1 m/s) [43], denoted by large regression angle and predicted by the numerical model [116] (Fig. 7e). Therefore, as the oxygen concentration increases, the laminar burning velocity increases, so the transition occurs at a higher opposed flow velocity [43,117].

As the flame height increases with the fuel size or burning area, eventually, the flame-induced buoyant flow becomes large enough to trigger the StR transition and push the flame into the wake region, so the observed downward flame motion no longer varies with the fuel size [118,119]. For charring materials, a wake flame is less stable; instead, smoldering spread tends to continuously regress the fuel [35,102]. The StR transition has been observed in the narrow channel apparatus, where the flame hides in the groove of thick fuel [50], and inside the porous fuel bed without spread [120], but has not yet been observed in microgravity. The fuel shape and curvature that enables a small-flow wake region (e.g. Fig. 3a) can promote StR transition.

For liquid fuels and thermoplastic fuels (e.g. PE and PS) which melt in a fire, the motion of liquid/molten fuel also plays a vital role in flame spread, such as in façade fires [122] and wire fires [123] (Fig. 7f). Flame spread over a moving liquid fuel and in flooring has not been well investigated [9]. For the burning of thermoplastic fuel, Kobayashi *et al*. [23,121] found that the rate of dripping flow dominates the rate of downward flame spread over the wire, and the cooling of the dripping front by the metal core and airflow can slow down the flame spread. Williams [1] predicted the downward spread rate of thermoplastic materials to be controlled by the force balance between surface tension and gravity of dripping, which needs more verification by experiment or numerical simulation. For opposed flame spread over liquid fuel, enormous wind speed may lead to a concurrent liquid flow that outspends the opposed flame spread, which is worthy of further investigation.

3.2. Smoldering-to-Flaming (StF) Transition

The phenomenon of smoldering-to-flaming (StF) transition is a quick initiation of homogenous gas-phase ignition preceded by smoldering combustion under an excessive oxygen supply (Fig. 8a), as recently reviewed in [124]. After the transition, the homogenous oxidation of the flame (Eq. 3b) will consume most of the oxygen due to faster chemistry, meanwhile smothering the heterogeneous oxidation of smoldering (Eq. 3c). Therefore, the *StF transition is also a type of smoldering extinction*, while the special co-existence of homogenous and heterogeneous oxidations (glowing combustion) will be discussed in the next section.

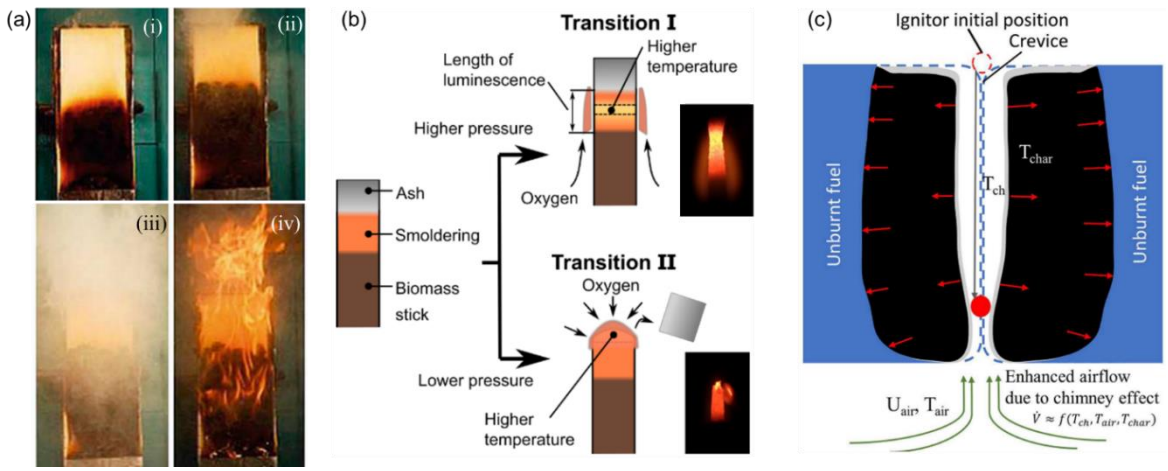

Fig. 8. Smoldering-to-flaming (StF) transition, (a) PU foam [125], (b) incense under different pressures [126], and (c) the role of chimney effect for internal smoldering [37,124].

The StF transition can take place in both opposed flow (trailing edge) and concurrent flow (leading edge) [127], so it is insensitive to the flow direction. One primary reason is that when the oxygen supply is excessive, smoldering can spread toward all possible directions to increase the burning area [128], as

illustrated in Fig. 1(b). Compared to concurrent smoldering, a larger airflow velocity is often needed for StF transition in the opposed mode [127]. This may be a result of the lower smoldering temperature in opposed smoldering spread, which needs further verification. It is hypothesized that the high-temperature char oxidation could pilot the pyrolysis gas mixture to cause the StF transition [129]. Although the secondary char oxidation with a different chemistry is also proposed [130,131], latest simulations showed that 1-step char oxidation could predict the StF transition [132]. Due to the strong gas-solid interaction, the StF can also be equally explained as a gas-phase auto-ignition above the hot char-oxidation (glowing) surface, but the complex fuel chemistry prevents an in-depth interpretation.

Like flame spread, the buoyant flow also enhances the oxygen supply to surface smoldering spread. As the pressure decreases, the propensity of StF transition decreased under the reduced buoyant flow [103,104], as illustrated in Fig. 8(b). The chimney effect is considered as the driving force for the StF transition for upholstered foam material [37] (Fig. 8c). For underground coal fires, a deeper smoldering fire has a greater chimney effect, so that extinction due to smothering will not occur [133]. Moreover, the larger upward buoyant flow will drag more air to feed deep-layer coal fires and trigger the StF transition near the free surface. Compared to the flow velocity and pressure, the StF transition is more sensitive to oxygen concentration [103,104], which highlights the critical role of oxidation kinetics.

For free-surface smoldering on a low-permeability fuel, a large flow velocity (1~5 m/s [40,124]) is needed for the StF transition, because the oxygen can only diffuse from the boundary layer to the porous burning region. For the internal smoldering spread, a much smaller airflow velocity (~0.1 m/s) within the porous bed is sufficient to trigger the StF transition [134,135]. Nevertheless, the smoldering temperature could also decrease with flow speed before StF [136]. So far, the physical meaning of the minimum flow velocity or flowrate for StF transition is still poorly understood. One requirement for the StF transition is that *the overall oxygen supply within and outside the porous fuel bed should be sufficient to maintain a flame*; otherwise, there would be only a local flash. For all existing experiments, this requirement is usually satisfied, because of the excessive wind or the flame-induced buoyant flow. Nevertheless, there should be (1) a minimum flowrate and pore size to maintain a flame inside the porous fuel that overcomes all heat losses through solid (like Fig. 3e), and (2) another minimum system flowrate for sustaining a flame outside the low-permeability fuel after transition. These critical parameters could be further studied in well-designed ground and microgravity experiments [56] and by numerical simulations.

3.3. Glowing Spread

Glowing is a widely observed phenomenon on the solid surface which is hot enough to emit visible light, such as in non-reactive solid (e.g. coil heater and incandescent lamp) and reactive solid (e.g. burning incense [35], wood [137], hot charcoal [29], and welding metal sparks [138]), as illustrated in Fig. 9(a-d). In terms of the burning of organic solid fuels, *glowing combustion* is a surface oxidation process of solid fuel accompanied by incandescence. Therefore, glowing combustion can be viewed as an "intense smoldering combustion" and often used as a synonym of smoldering in the literature [97]. Boonmee and Quintiere [139] found that at irradiation > 40 kW/m^2, flaming auto-ignition occurred for wood, while at irradiation < 40 kW/m^2, glowing (or smoldering) ignition would occur. Later, they hypothesized that the glowing ignition process was first kinetic-controlled [1] when the surface temperature was lower than 673 K, and then diffusion-controlled at higher temperature [140].

Ohlemiller [10] speculated that gas-phase oxidative reactions might not be dominant compared to surface reactions in smoldering, but they may play a "significant supplementary role." Nevertheless, because of the high surface temperature in glowing (>900 K), homogenous gas-phase reactions can play a vital role and even sustain a flame above the smoldering surface. In fact, if the heat release from gas-phase homogenous reactions (Eq. 3b) exceeds that from heterogenous reactions (Eq. 3c), calling it either smoldering or flaming becomes inappropriate; instead, glowing is used to highlight the co-existence of homogenous and heterogenous oxidations. Compared to smoldering, glowing combustion has some unique features due to the pronounced radiation heat transfer and intense gas-phase reactions interacting with surface reactions. Today, gas-phase reactions are usually neglected in numerical models for steady-state glowing or smoldering combustion [39,142,143], except for predicting the StF transition [131]. The radiation heat transfer inside the smoldering

porous media is also not well studied, but it plays an important role in glowing spread because of a higher solid surface temperature.

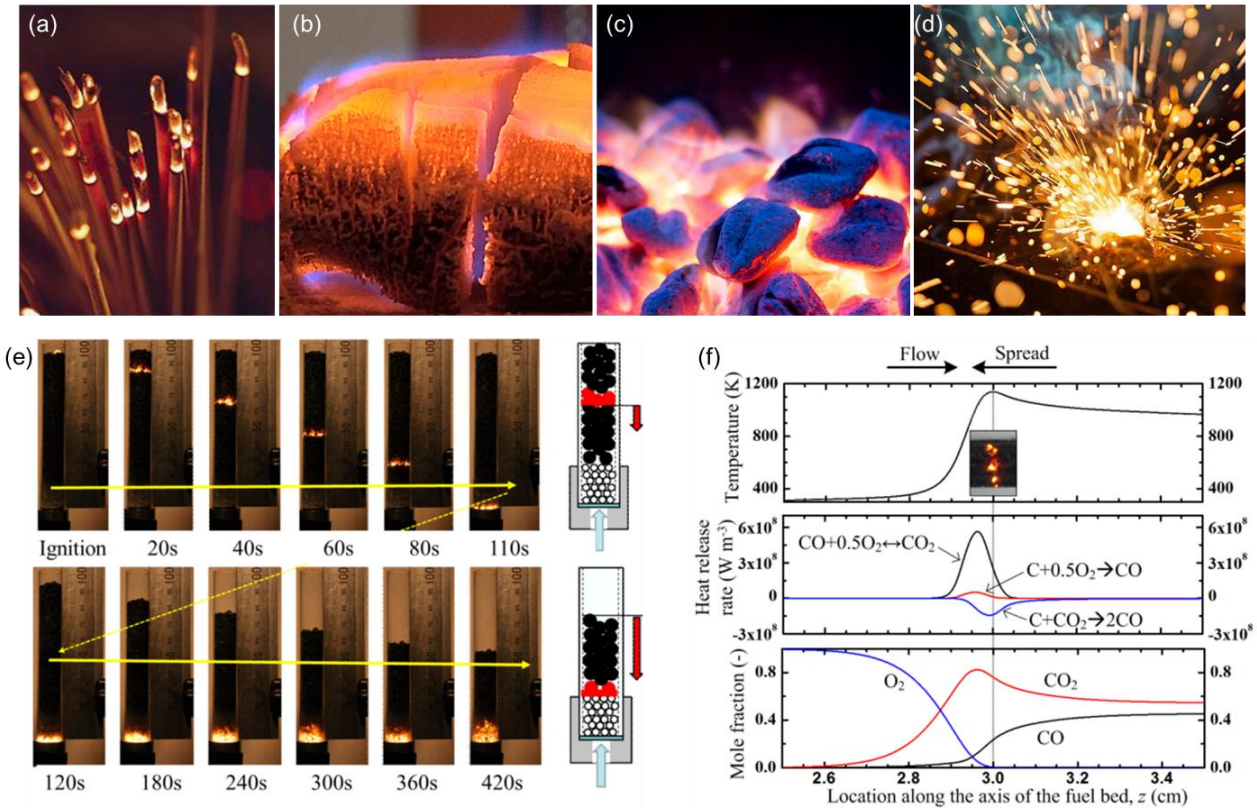

Fig. 9. Glowing phenomena, (a) burning incense [35], (b) wood [137], (c) hot charcoal, and (d) welding metal sparks; glowing combustion in a packed bed of activated carbon particles (e) experiment [120], and (f) simulated profiles of temperature, reaction heat release rate, and species mole fraction [141].

Recently, Nakamura *et al.* [120] showed a glowing spread in a vertically orientated packed bed of activated carbon particles with an upward oxidant flow of CO_2/O_2 mixtures. Following ignition at the top of the bed, an opposed glowing front was formed and propagated downwards with a visible incandescence (Fig. 9e). After reaching the bottom, it transitioned to the concurrent (regression) mode. Due to negligible volatile matter content (< 5%) in activated carbon, there is neither pyrolysis nor evaporation. The dominant gas-phase reaction must be the oxidation of CO that is produced from smoldering. In other words, in this glowing spread, heterogenous smoldering combustion is a necessary condition for homogenous flaming reactions.

To quantify the competition between homogenous (especially the CO oxidation) and heterogeneous oxidation in the glowing surface, Gao *et al.* [141] simulated the profiles of a glowing front with a transient 2D model (Fig. 9f), where the predicted glowing temperature was above 1100 K, and the heat release rate of CO oxidation dominates over both the C-O_2 and CO_2-O_2 surface reaction. Thus, both the surface oxidation and CO oxidation are compulsory to sustain the glowing spread in these high fixed-carbon content materials. A similar process is expected for glowing incense [35], wood [137], and charcoal (Fig. 9a-c). Glowing is a steady-state intermediate in-between smoldering and flaming, different from the unstable StF transition. Therefore, a well-controlled glowing process provides (1) an ideal bench scheme for investigating the mechanism of StF transition, and (2) a method for the in-situ removal of toxic emissions from smoldering.

It is worth noting that the propagation of the combustion front observed in the packed bed of biomass [144–148] and solid waste [41] can also be categorized as glowing spread, given the co-existence of hetero- and homogeneous oxidations. The biomass combustion community often terms the process as “ignition front propagation”, which shares a similar meaning of “fire spread” in the fire community. Compared to activated carbon particles, biomass can have a volatile content up to 70 wt.%. Therefore, besides CO oxidation, oxidation of volatiles in the gas phase should also play an essential role in sustaining the glowing spread. The rich literature on biomass combustion could provide valuable information to understand the glowing fire phenomena, which deserves a further systematic review.

3.4. Blowoff

Blowoff of opposed flame spread (Fig. 10a) has been studied over the last 50 years with a large number of experiments, theoretical analysis, and numerical simulations, as reviewed in detail by Wichman [6]. Essentially, some *Da** in Eq. (9), depending on the fire configuration and environmental parameters, can provide a reasonable explanation for most blowoff phenomena. For example, the blowoff velocity for opposed flow increased with the oxygen concentration [19,149], because of the increased oxidation rate or the decreased reaction time. This section briefly reviews a few unique and unsolved blowoff phenomena.

Because a candle-like flame can induce a buoyant flow with the velocity at about 30 cm/s, if the oxygen concentration is reduced, the flame will eventually be blown off by the self-induced buoyant flow (Fig. 10b). In other words, the measured LOC on Earth via standard tests [150] is the oxygen level when self-blowoff by buoyant flow occurs [53] (also see Fig. 4e). The self-blowoff may become easier, if the fuel becomes thinner [43,151]; the buoyancy is enhanced [152]; or a charring fuel like wood is used. Reducing the pressure, blowoff under forced flow occurs readily, while self-blowoff becomes difficult, thus further investigation is needed to clarify the self-blowoff mechanism. Near blowoff, cooling by solid-phase conduction and radiation becomes more important, such as in wire fires [21,44] and under microgravity conditions [106,153]. Thus, the gas-phase *Da* alone may not be sufficient to explain the blowoff phenomena. Studies on the blowoff of flame spreading on liquid fuels are still limited [9,24,25], and thoroughly exploring the influence of liquid fuel type and conditions of pool and environment (e.g. pressure and oxygen level) on blowoff is desired.

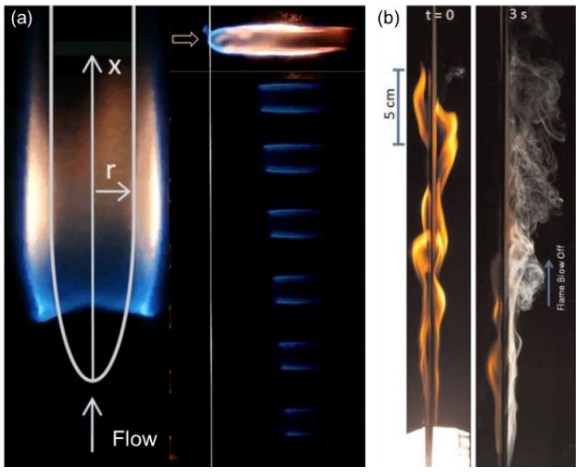

Fig. 10. (a) The post-stagnation flame blowoff in microgravity [153], and (b) self-blowoff of paper flame [151].

For blowoff of smoldering, the related research is very limited. Palmer [28] found that surface smoldering could be blown off under an opposed wind of 7 m/s, but not under a concurrent wind up to 10 m/s (Fig. 2b). Matsui and Tsuji [154,155] proposed a surface *Da* to characterize heterogenous oxidation of solid carbon within a flame sheet. In general, blowing off smoldering is more difficult than flaming, but it should be easier to achieve under a lower pressure and oxygen level, which needs further systematic demonstration. As the wind speed increases, it is expected to first observe the StF transition, and then a second transition from flaming blowoff to smoldering due to the easier blowoff of flaming. In short, there are still many unknowns about blowoff, such as microgravity flames, micro-flames, and flames within porous beds, and more work is needed to fulfill these knowledge gaps.

4. Conclusions and Perspectives

The continuous research on fire spread over the last 50 years has significantly improved our understanding of fire phenomena. This review focuses on new and unique fire phenomena under limited and excessive oxygen supply that are still not fully understood. Under limited-oxygen supply, the generally ignored effects of radiation, solid-phase heat transfer, and chemical reactions in fire spread are highlighted. The near-limit spread of flaming and smoldering are compared throughout the review, as they share many similarities in different spread regimes and the fingering-spread process. Under excessive oxygen supply, two transitions, namely, the smoldering-to-flaming (StF) transition and the spread-to-regression (StR) transition, are reviewed comprehensively. Efforts have been made to clarify the difference between fire spread and fuel regression in both flaming and smoldering, which have been often misused in the community. For the first time, recent research activities regarding glowing spread, which is an intermediate status in between flaming and smoldering, is summarized.

Although a lot of effort has already been devoted to investigating these near-limit fire spread behaviors, there is a great deal of room for an understanding the physics behind them, especially in following aspects:

(1) Surface re-radiation and flame radiation at different near-extinction conditions need quantification;

(2) Limiting conditions of fingering spread need to include parameters of system and further validations;

(3) Physical meaning behind the LOC of smoldering requires further clarification;

(4) Attention is needed for phase-change processes of thermoplastics at near-limit flame spread;

(5) Minimum flowrate and pore size to sustain flaming or glowing spread inside the porous fuel, as well as to trigger the StF transition, should be determined;

(6) Homogeneous oxidation of CO and volatiles in glowing spread should be systematically studied to define the boundary between flaming and smoldering;

(7) Blowoff of smoldering is still poorly understood, so that extensive investigations are desired.

In general, new microgravity experiments and numerical simulations on glowing, blowoff, and StF and StR transitions are helpful. Additional effort is beneficial for the usage and extrapolation of the experimental, theoretical, and computational combustion and fire research that has been completed to improve the fire safety in practice, because the full benefit of research cannot be realized without solving real engineering issues.

Acknowledgments

This work was supported by the National Natural Science Foundation of China (No. 51876183, 51806230) and ZJU SKLCEU Open Fund (2018012). The comments from Matsuoka Tsuneyoshi (Toyohashi Tech) and the assistance from Shaorun Lin and Yanhui Liu (PolyU) are acknowledged. XH offers his most sincere appreciation to Profs. Forman Williams, Carlos Fernandez-Pello, Guillermo Rein, Michael Gollner, and Yuji Nakamura, who have taught him the fundamentals of combustion and fire, as well as, the IAFSS that invited this review as part of the *Proulx Early Career Award*.

References

[1] Williams FA. Mechanisms of fire spread. Symposium (International) on Combustion 1977;16:1281–94.
[2] Emmons HW. Fire in the forest. Fire Research Abstracts and Reviews 1963;5:163–78.
[3] Friedman R. A survey of knowledge about idealized fire spread over surfaces. Fire Research Abstracts and Reviews 1968;10.
[4] Fernandez-Pello C, Hirano T. Controlling Mechanisms of Flame Spread. Combustion Science and Technology 1983;32:1–31.
[5] Loh H-TT, Fernandez-Pello AC, Fernandez-pello CA, Fernandez-Pello AC, Fernandez-pello CA. A study of the controlling mechanisms of flow assisted flame spread. Twentieth Symposium (International) on Combustion 1984;20:1575–82.
[6] Wichman IS. Theory of opposed-flow flame spread. Progress in Energy and Combustion Science 1992;18:553–93.
[7] Fernandez-Pello CA. The solid phase. In: Cox G, editor. Combustion fundamentals of fire, San Diego: Academic Press INC.; 1995, p. 31–100.
[8] Gollner MJ, Miller CH, Tang W, Singh A V. The effect of flow and geometry on concurrent flame spread. Fire Safety Journal 2017;91:68–78.
[9] Ross HD. Ignition of and flame spread over laboratory-scale pools of pure liquid fuels. Progress in Energy and Combustion Science 1994;20:17–63.
[10] Ohlemiller TJ. Modeling of smoldering combustion propagation. Progress in Energy and Combustion Science 1985;11:277–310.
[11] Cheney NP, Gould JS, Catchpole WR. Prediction of fire spread in grasslands. International Journal of Wildland Fire 1998;8:1–13.
[12] Quintiere J. Fundamentals of Fire Phenomena. London: John Wiley & Sons, Ltd; 2006.
[13] Lu Y, Huang X, Hu L, Fernandez-Pello C. Concurrent Flame Spread and Blow-Off Over Horizontal Thin Electrical Wires. Fire Technology 2018;55:193–209.
[14] Finney MA, Cohen JD, Forthofer JM, McAllister SS, Gollner MJ, Gorham DJ, et al. Role of buoyant flame dynamics in wildfire spread. Proceedings of the National Academy of Sciences 2015;112:9833–8.
[15] Gollner MJ, Huang X, Cobian J, Rangwala AS, Williams FA. Experimental study of upward flame spread of an inclined fuel surface. Proceedings of the Combustion Institute 2013;34:2531–8.
[16] Wichman IS, Williams FA, Glassman I. Theoretical aspects of flame spread in an opposed flow over flat surfaces of solid fuels. Symposium (International) on Combustion 1982;19:835–45.
[17] Delichatsios MA. Relation of opposed flow (creeping) flame spread with extinction/ignition. Combustion and Flame 2003;135:441–7.

[18] Delichatsios M a. Creeping flame spread: Energy balance and application to practical materials. Symposium (International) on Combustion 1996;26:1495–503.
[19] Fernandez-Pello AC, Ray SR, Glassman I. Flame spread in an opposed forced flow: the effect of ambient oxygen concentration. Symposium (International) on Combustion 1981;18:579–89.
[20] De Ris JN. Spread of a laminar diffusion flame. Symposium (International) on Combustion 1969;12:241–52.
[21] Nakamura Y, Yoshimura N, Matsumura T, Ito H, Fujita O. Opposed-wind Effect on Flame Spread of Electric Wire in Sub-atmospheric Pressure. Journal of Thermal Science and Technology 2008;3:430–41.
[22] Bhattacharjee S, Tran W, Laue M, Paolini C, Nakamura Y. Experimental validation of a correlation capturing the boundary layer effect on spread rate in the kinetic regime of opposed-flow flame spread. Proceedings of the Combustion Institute 2015;35:2631–8.
[23] Kobayashi Y, Konno Y, Huang X, Nakaya S, Tsue M, Hashimoto N, et al. Effect of insulation melting and dripping on opposed flame spread over laboratory simulated electrical wires. Fire Safety Journal 2018;95:1–10.
[24] Suzuki T, Hirano T. Flame propagation across a liquid fuel in an air stream. Symposium (International) on Combustion 1982;19:877–84.
[25] Li M, Wang C, Li Z, Yang S, Fukumoto K, Fan C. Combustion and flame spreading characteristics of diesel fuel with forced air flows. Fuel 2018;216:390–7.
[26] Ito A, Kashiwagi T. Characterization of flame spread over PMMA using holographic interferometry sample orientation effects. Combustion and Flame 1988;71:189–204.
[27] Emberley R, Inghelbrecht A, Yu Z, Torero JL. Self-extinction of timber. Proceedings of the Combustion Institute 2017;36:3055–62.
[28] Palmer KN. Smouldering combustion in dusts and fibrous materials. Combustion and Flame 1957;1:129–54.
[29] Rein G. Smoldering Combustion. SFPE Handbook of Fire Protection Engineering 2014;2014:581–603.
[30] Chao CYH, Wang JH. Comparison of the thermal decomposition behavior of a non-fire retarded and a fire retarded flexible polyurethane foam with phosphorus and brominated additives. Journal of Fire Sciences 2001;19:137–56.
[31] Huang X, Rein G. Thermochemical conversion of biomass in smouldering combustion across scales: The roles of heterogeneous kinetics, oxygen and transport phenomena. Bioresource Technology 2016;207:409–21.
[32] Lin S, Huang X. Quenching of Smoldering: Effect of Wall Cooling on Extinction. Proceedings of the Combustion Institute (Accepted) 2020.
[33] Law CK. Combustion physics. Cambridge university press; 2010.
[34] Zanoni MAB, Torero JL, Gerhard JI. Delineating and explaining the limits of self-sustained smouldering combustion. Combustion and Flame 2019;201:78–92.
[35] Yamazaki T, Matsuoka T, Nakamura Y. Near-extinction behavior of smoldering combustion under highly vacuumed environment. Proceedings of the Combustion Institute 2019;37:4083–90.
[36] Song Z, Wu D, Jiang J, Pan X. Thermo-solutal buoyancy driven air flow through thermally decomposed thin porous media in a U-shaped channel: Towards understanding persistent underground coal fires. Applied Thermal Engineering 2019;159:113948.
[37] Ogle RA, Schumacher JL. Fire patterns on upholstered furniture: Smoldering versus flaming combustion. Fire Technology 1998;34:263–5.
[38] Huang X, Restuccia F, Gramola M, Rein G. Experimental study of the formation and collapse of an overhang in the lateral spread of smouldering peat fires. Combustion and Flame 2016;168:393–402.
[39] Huang X, Rein G. Upward-and-downward spread of smoldering peat fire. Proceedings of the Combustion Institute 2019;37:4025–33.
[40] Xie Q, Zhang Z, Lin S, Qu Y, Huang X. Smoldering of high-density cotton bale under concurrent wind. Fire Technology 2020.
[41] Shin D, Choi S. The combustion of simulated waste particles in a fixed bed. Combustion and Flame 2000;121:167–80.
[42] Fernandez-Pello AC. Wildland fire spot ignition by sparks and firebrands. Fire Safety Journal 2017;91:2–10.
[43] Huang X, Link S, Rodriguez A, Thomsen M, Olson S, Ferkul P, et al. Transition from opposed flame spread to fuel regression and blow off: Effect of flow, atmosphere, and microgravity. Proceedings of the Combustion Institute 2019;37:4117–26.
[44] Takahashi S, Ito H, Nakamura Y, Fujita O. Extinction limits of spreading flames over wires in microgravity. Combustion and Flame 2013;160:1900–2.
[45] Kashiwagi T, Mcgrattan KB, Olson SL, Fujita O, Kikuchi M, Ito K. Effects of slow wind on localized radiative ignition and transition to flame spread in microgravity. Combustion 1996;26:1345–52.

[46] Olson SL, Kashiwagi T, Fujita O, Kikuchi M, Ito K. Experimental observations of spot radiative ignition and subsequent three-dimensional flame spread over thin cellulose fuels. Combustion and Flame 2001;125:852–64.
[47] Wu C, Huang X, Wang S, Zhu F, Yin Y. Opposed-flow flame spread over cylindrical fuel under oxygen-enriched microgravity environment. Fire Technology 2020;56:71–89.
[48] Vetturini A, Cui W, Liao YT, Olson S, Ferkul P. Flame Spread Over Ultra-thin Solids: Effect of Area Density and Concurrent-Opposed Spread Reversal Phenomenon. Fire Technology 2020.
[49] Robert A. Altenkirch, Lin Tang, Kurt Sacksteder, Subrata Bhattacharjee MAD, Altenkirch RA, Tang L, Sacksteder K, Bhattacharjee S, Delichatsios MA. Inherently unsteady flame spread to extinction over thick fuels in microgravity. Proceedings of the Combustion Institute 1998;27:2515–24.
[50] Zhu F, Lu Z, Wang S. Flame Spread and Extinction Over a Thick Solid Fuel in Low-Velocity Opposed and Concurrent Flows. Microgravity Science and Technology 2016;28:87–94.
[51] Ross HD. Microgravity combustion : fire in free fall. Academic Press; 2001.
[52] Friedman R. Fire Safety Spacecraft in the Low-Gravity Environment. 1999.
[53] Fujita O. Solid combustion research in microgravity as a basis of fire safety in space. Proceedings of the Combustion Institute 2015;35:2487–502.
[54] Huang X, Nakamura Y, Urban DL. Introduction to Special Issue on Spacecraft Fire Safety. Fire Technology 2020;56:1–4.
[55] Nakamura Y, Yoshimura N, Matsumura T, Ito H, Fujita O. Flame Spread over Polymer-Insulated Wire in Sub-Atmospheric Pressure : Similarity to Microgravity Phenomena. In: Saito K, editor. Progress in Scale Modeling, Springer; 2008, p. 17–27.
[56] Olson SL, Miller FJ, Jahangirian S, Wichman IS. Flame spread over thin fuels in actual and simulated microgravity conditions. Combustion and Flame 2009;156:1214–26.
[57] Mell WE, Kashiwagi T. Dimensional effects on the transition from ignition to flame spread in microgravity. Symposium (International) on Combustion 1998;27:2635–41.
[58] Olson SL. Mechanisms of Microgravity Flame Spread Over a Thin Solid Fuel: Oxygen and Opposed Flow Effects. Combustion Science and Technology 1991;76:233–49.
[59] Takahashi S, Borhan MAF Bin, Terashima K, Hosogai A, Kobayashi Y. Flammability limit of thin flame retardant materials in microgravity environments. Proceedings of the Combustion Institute 2019;37:4257–65.
[60] Link S, Huang X, Fernandez-Pello C, Olson S, Ferkul P. The Effect of Gravity on Flame Spread over PMMA Cylinders. Scientific Reports 2018;8:120.
[61] Olson SL, Hegde U, Bhattacharjee S, Deering JL, Tang L, Altenkirch RA. Sounding rocket microgravity experiments elucidating diffusive and radiative transport effects on flame spread over thermally thick solids. Combustion Science and Technology 2004;176:557–84.
[62] Wu C, Sun P, Wang X, Huang X, Wang S. Flame Extinction of Spherical PMMA in Microgravity: the Effect of Solid Diameter, Conduction and Radiation. Microgravity Science and Technology [under Review] 2020.
[63] Mell WE, Olson SL, Kashiwagi T. Flame spread along free edges of thermally thin samples in microgravity. Proceedings of the Combustion Institute 2000;28:2843–9.
[64] T'ien JS. Diffusion flame extinction at small stretch rates: The mechanism of radiative loss. Combustion and Flame 1986;65:31–4.
[65] Daguse T, Croonenbroek T, Rolon JC, Darabiha N, Soufiani A. Study of radiative effects on laminar counterflow H2/O2/N2 diffusion flames. Combustion and Flame 1996;106:271–87.
[66] Maruta K, Yoshida M, Guo H, Ju Y, Niioka T. Extinction of low-stretched diffusion flame in microgravity. Combustion and Flame 1998;112:181–7.
[67] Bhattacharjee S, Ayala R, Wakai K, Takahashi S. Opposed-flow flame spread in microgravity-theoretical prediction of spread rate and flammability map. Proceedings of the Combustion Institute 2005;30:2279–86.
[68] Bhattacharjee S, Simsek A, Miller F, Olson S, Ferkul P. Radiative, thermal, and kinetic regimes of opposed-flow flame spread: A comparison between experiment and theory. Proceedings of the Combustion Institute 2017;36:2963–9.
[69] Olson SL, Ferkul P V. Microgravity flammability boundary for PMMA rods in axial stagnation flow: Experimental results and energy balance analyses. Combustion and Flame 2017;180:217–29.
[70] Bhattacharjee S, Dong K. A numerical investigation of radiation feedback in different regimes of opposed flow flame spread. International Journal of Heat and Mass Transfer 2020;150:119358.
[71] Takahashi S, Nagata T, Hotta M, Bhattacharjee S, Ihara T, Wakai K. Behavior of Flame Spread on Thin PMMA near Extinction Limit at Low Oxygen Level. Trans JSASS Aerospace Tech Japan 2012;10:9–13.
[72] Takahashi S, Kondou M, Wakai K, Bhattacharjee S. Effect of radiation loss on flame spread over a thin PMMA sheet in microgravity. Proceedings of the Combustion Institute 2002;29:2579–86.
[73] Carmignani L, Celniker G, Bhattacharjee S. The Effect of Boundary Layer on Blow-Off Extinction in

Opposed-Flow Flame Spread over Thin Cellulose: Experiments and a Simplified Analysis. Fire Technology 2017;53:967–82.
[74] Zhang Y, Ronney PD, Roegner EV, Greenberg JB, Tj- A. Lewis Number Effects on Flame Spreading Over Thin Solid Fuels. Combustion and Flame 1992;83:71–83.
[75] Zik O, Moses E. Fingering instability in combustion: An extended view. Physical Review E - Statistical Physics, Plasmas, Fluids, and Related Interdisciplinary Topics 1999;60:518–31.
[76] Zik O, Moses E. Fingering instability in solid fuel combustion: The characteristic scales of the developed state. Symposium (International) on Combustion 1998;27:2815–20.
[77] Zik O, Olami Z, Moses E. Fingering Instability in Combustion. Physical Review Letters 1998;81:3868–71.
[78] Olson SL, Baum HR, Kashiwagi T. Finger-like smoldering over thin cellulosic sheets in microgravity. Symposium (International) on Combustion 1998;27:2525–33.
[79] Matsuoka T, Nakashima K, Nakamura Y, Noda S. Appearance of flamelets spreading over thermally thick fuel. Proceedings of the Combustion Institute 2017;36:3019–26.
[80] Zhu F, Lu Z, Wang S, Yin Y. Microgravity diffusion flame spread over a thick solid in step-changed low-velocity opposed flows. Combustion and Flame 2019;205:55–67.
[81] Malchi JY, Yetter RA, Son SF, Risha GA. Nano-aluminum flame spread with fingering combustion instabilities. Proceedings of the Combustion Institute 2007;31 II:2617–24.
[82] Veiga-López F, Martínez-Ruiz D, Fernández-Tarrazo E, Sánchez-Sanz M. Experimental analysis of oscillatory premixed flames in a Hele-Shaw cell propagating towards a closed end. Combustion and Flame 2019;201:1–11.
[83] Veiga-López F, Kuznetsov M, Martínez-Ruiz D, Fernández-Tarrazo E, Grune J, Sánchez-Sanz M. Unexpected Propagation of Ultra-Lean Hydrogen Flames in Narrow Gaps. Physical Review Letters 2020;124:174501.
[84] Olson S, Miller F, Wichman I. Characterizing fingering flamelets using the logistic model. Combustion Theory and Modelling 2006;10:323–47.
[85] Wang S, Wang S, Zhu K, Xiao Y, Lu Z. Near Quenching Limit Instabilities of Concurrent Flame Spread over Thin Solid Fuel. Combustion Science and Technology 2016;188:451–71.
[86] Kuwana K, Suzuki K, Tada Y, Kushida G. Effective Lewis number of smoldering spread over a thin solid in a narrow channel. Proceedings of the Combustion Institute 2017;36:3203–3210.
[87] Kagan L, Sivashinsky G. Pattern formation in flame spread over thin solid fuels. Combustion Theory and Modelling 2008;12:269–81.
[88] Ijioma ER, Muntean A, Ogawa T. Effect of material anisotropy on the fingering instability in reverse smoldering combustion. International Journal of Heat and Mass Transfer 2015;81:924–38.
[89] Ijioma ER, Muntean A, Ogawa T. Stratified turbulent Bunsen flames: flame surface analysis and flame surface density modelling. Combustion Theory and Modelling 2013;17:185–223.
[90] Uchida Y, Kuwana K, Kushida G. Experimental validation of Lewis number and convection effects on the smoldering combustion of a thin solid in a narrow space. Combustion and Flame 2015;162:1957–63.
[91] Kuwana K, Suzuki K, Tada Y, Kushida G. Effective Lewis number of smoldering spread over a thin solid in a narrow channel. Proceedings of the Combustion Institute 2017;36:3203–10.
[92] Funashima K, Masuyama A, Kuwana K, Kushida G. Opposed-flow flame spread in a narrow channel: Prediction of flame spread velocity. Proceedings of the Combustion Institute 2019;37:3757–65.
[93] Lu Z, Dong Y. Fingering instability in forward smolder combustion. Combustion Theory and Modelling 2011;15:795–815.
[94] Kumar P, Kumar A, Karpov A. Near limit flame spread over thin solid fuels in a low convective microgravity environment. Proceedings of the Combustion Institute 2019;37:3825–32.
[95] Lin S, Sun P, Huang X. Can peat soil support a flaming wildfire? International Journal of Wildland Fire 2019;28:601–13.
[96] Bar-Ilan A, Rein G, Walther DC, Fernandez-Pello AC, Torero JL, Urban DL. The effect of buoyancy on opposed smoldering. Combustion Science and Technology 2004;176:2027–55.
[97] Rein G. Smouldering Combustion Phenomena in Science and Technology. International Review of Chemical Engineering 2009;1:3–18.
[98] Torero JL, Deffend D, Kitano M. Downward Smolder of Polyurethane Foam. Fire Safety Science 1994;4:409–20.
[99] Cohen IM, Kundu PK. Fluid Mechanics. Elsevier Science; 2007.
[100] Babrauskas V. Ignition Handbook. Issaquah, WA: Fire Science Publishers/Society of Fire Protection Engineers; 2003.
[101] Walther DC, Carlos Fernandez-Pello A, Urban DL. Small-scale smoldering combustion experiments in microgravity. Proceedings of the Combustion Institute 1996;26:1361–8.
[102] Moussa N a., Toong TY, Garris C a. Mechanism of smoldering of cellulosic materials. Symposium (International) on Combustion 1977;16:1447–57.

[103] Ortiz-Molina MG, Toong T-Y, Moussa NA, Tesoro GC. Smoldering combustion of flexible polyurethane foams and its transition to flaming or extinguishment. Symposium (International) on Combustion 1979;17:1191–200.
[104] Yamazaki T, Matsuoka T, Li Y, Nakamura Y. Applicability of a Low-Pressure Environment to Investigate Smoldering Behavior Under Microgravity. Fire Technology 2020.
[105] Frey AE, T'ien J. Near-Limit Flame Spread Over Paper Samples. Combustion and Flame 1976;267:257–67.
[106] Urban DL, Ferkul P, Olson S, Ruff GA, James ST, Liao YT, et al. Flame Spread: Effects of Microgravity and Scale. Combustion and Flame 2018;199:1–22.
[107] Hadden RM, Rein G, Belcher CM. Study of the competing chemical reactions in the initiation and spread of smouldering combustion in peat. Proceedings of the Combustion Institute 2013;34:2547–53.
[108] Belcher CM, Yearsley JM, Hadden RM, Mcelwain JC, Rein G. Baseline intrinsic flammability of Earth ' s ecosystems estimated from paleoatmospheric oxygen over the past 350 million years. Proceedings of the National Academy of Sciences 2010;107:22448–22453.
[109] Huang X, Rein G. Interactions of Earth's atmospheric oxygen and fuel moisture in smouldering wildfires. Science of the Total Environment 2016;572:1440–6.
[110] Wang H, van Eyk PJ, Medwell PR, Birzer CH, Tian ZF, Possell M. Effects of Oxygen Concentration on Radiation-Aided and Self-sustained Smoldering Combustion of Radiata Pine. Energy & Fuels 2017;31:8619–30.
[111] Schmidt M, Lohrer C, Krause U. Self-ignition of dust at reduced volume fractions of ambient oxygen. Journal of Loss Prevention in the Process Industries 2003;16:141–7.
[112] Malow M, Krause U. Smouldering combustion of solid bulk materials at different volume fractions of oxygen in the surrounding gas. Fire Safety Science 2008;9:303–14.
[113] Hashimoto N, Watanabe S, Nagata H, Totani T, Kudo I. Opposed-flow flame spread in a circular duct of a solid fuel: Influence of channel height on spread rate. Proceedings of the Combustion Institute 2002;29:245–50.
[114] Komizu K, Saito Y, Tsuji A, Nagata H. Experimental Investigation of the Continuous Transition of Flame-Spreading near the Blow-Off Limit. Journal of Combustion 2020:3187694.
[115] Delzeit T, Carmignani L, Matsuoka T, Bhattacharjee S. Influence of edge propagation on downward flame spread over three-dimensional PMMA samples. Proceedings of the Combustion Institute 2019;37:3203–9.
[116] Kumar A, T'ien JS. A computational study of low oxygen flammability limit for thick solid slabs. Combustion and Flame 2006;146:366–78.
[117] Sibulkin M, Little MW. Propagation and Extinction of Downward Burning Fires. Combustion and Flame 1978;31:197–208.
[118] Fernández-Pello C, Williams FA. A theory of laminar flame spread over flat surfaces of solid combustibles. Combustion and Flame 1977;28:251–77.
[119] Carmignani L, Rhoades B, Bhattacharjee S. Correlation of Burning Rate with Spread Rate for Downward Flame Spread Over PMMA. Fire Technology 2018;54:1–12.
[120] Nakamura Y, Yoshitome H, Yamazaki T, Matsuoka T, Gao J. Combustion of activated carbon particles part.1: Experimental investigation of the two distinctive burning modes in a packed bed. Energy Procedia 2019;158:2152–7.
[121] Kobayashi Y, Huang X, Nakaya S, Tsue M, Fernandez-Pello C. Flame spread over horizontal and vertical wires: The role of dripping and core. Fire Safety Journal 2017;91:112–22.
[122] Xie Q, Tu R, Wang N, Ma X, Jiang X. Experimental study on flowing burning behaviors of a pool fire with dripping of melted thermoplastics. Journal of Hazardous Materials 2014;267:48–54.
[123] Huang X, Nakamura Y. A Review of Fundamental Combustion Phenomena in Wire Fires. Fire Technology 2020;56:315–360.
[124] Santoso MA, Christensen EG, Yang J, Rein G. Review of the Transition From Smouldering to Flaming Combustion in Wildfires. Frontiers in Mechanical Engineering 2019;5.
[125] Putzeys O, Bar-Ilan A, Rein G, Fernandez-Pello a. C, Urban DL. The role of secondary char oxidation in the transition from smoldering to flaming. Proceedings of the Combustion Institute 2007;31:2669–76.
[126] Yamazaki T, Li Y, Matsuoka T, Salaimeh AA, Li T, Saito K. A Flaming Transition of Smoldering Thin-rod Biomass in Low Pressure. 12th Asia-Pacific Conference on Combustion, Fukuoka, Japan 1st -5th, July 2019, 2019.
[127] Ohlemiller TJ. Forced smolder propagation and the transition to flaming in cellulosic insulation. Combustion and Flame 1990;81:354–65.
[128] Wang S, Huang X, Chen H, Liu N. Interaction between flaming and smouldering in hot-particle ignition of forest fuels and effects of moisture and wind. International Journal of Wildland Fire 2017;26:71–81.
[129] Alexopoulos S, Drysdale DD. The transition from smouldering to flaming combustion. Fire and Materials 1988;13:37–44.
[130] Torero JL, Fernandez-Pello a. C. Natural convection smolder of polyurethane foam, upward propagation.

Fire Safety Journal 1995;24:35–52.
[131] Dodd AB, Lautenberger C, Fernandez-Pello C. Computational modeling of smolder combustion and spontaneous transition to flaming. Combustion and Flame 2012;159:448–61.
[132] Yang J, Liu N, Chen H, Gao W. Smoldering and spontaneous transition to flaming over horizontal cellulosic insulation. Proceedings of the Combustion Institute 2019;37:4073–81.
[133] Zeyang Song, Huang X, Kuenzer C, Zhu H, Jiang J, Pan X, et al. Chimney effect induced by smoldering fire in a U-shaped porous channel: A governing mechanism of the persistent underground coal fires. Process Safety and Environmental Protection 2020;136:136–47.
[134] Bar-Ilan A, Putzeys OM, Rein G, Fernandez-Pello AC, Urban DL. Transition from forward smoldering to flaming in small polyurethane foam samples. Proceedings of the Combustion Institute 2005;30:2295–302.
[135] Xie Q, Gao M, Huang X. Fire Risk and Behavior of Rice during the Convective Drying Process. Fire Safety Journal 2020.
[136] Yermán L, Wall H, Torero J, Gerhard JI, Cheng YL. Smoldering Combustion as a Treatment Technology for Feces: Sensitivity to Key Parameters. Combustion Science and Technology 2016;188:968–81.
[137] Lin S, Huang X, Gao J, Ji J. Extinction of Wood Fuels: A Near-limit Blue Flame Sustained above the Hot Smoldering Surface. Combustion and Flame [under Review] 2020.
[138] Liu Y, Urban JL, Xu C, Fernandez-Pello C. Temperature and motion tracking of metal spark sprays. Fire Technology 2019.
[139] Boonmee N, Quintiere JG. Glowing and flaming autoignition of wood. Proceedings of the Combustion Institute 2002;29:289–96.
[140] Boonmee N, Quintiere JG. Glowing ignition of wood: The onset of surface combustion. Proceedings of the Combustion Institute 2005;30 II:2303–10.
[141] Gao J, Xiaobin Qi, Zhang D, Matsuoka T, Nakamura Y. Propagation of glowing combustion front in a packed bed of activated carbon particles and the role of CO oxidation. Proceedings of the Combustion Institute (under Review) 2020.
[142] Rein G, Carlos Fernandez-Pello a., Urban DL. Computational model of forward and opposed smoldering combustion in microgravity. Proceedings of the Combustion Institute 2007;31:2677–84.
[143] He F, Behrendt F. Comparison of Natural Upward and Downward Smoldering Using the Volume Reaction Method. Energy & Fuels 2009;23:5813–20.
[144] Saastamoinen JJ, Taipale R, Horttanainen M, Sarkomaa P. Propagation of the ignition front in beds of wood particles. Combustion and Flame 2000;123:214–26.
[145] Porteiro J, Patiño D, Moran J, Granada E. Study of a fixed-bed biomass combustor: Influential parameters on ignition front propagation using parametric analysis. Energy and Fuels 2010;24:3890–7.
[146] Ryu C, Yang Y Bin, Khor A, Yates NE, Sharifi VN, Swithenbank J. Effect of fuel properties on biomass combustion: Part I. Experiments - Fuel type, equivalence ratio and particle size. Fuel 2006;85:1039–46.
[147] Yang Y Bin, Ryu C, Khor A, Yates NE, Sharifi VN, Swithenbank J. Effect of fuel properties on biomass combustion. Part II. Modelling approach - Identification of the controlling factors. Fuel 2005;84:2116–30.
[148] Porteiro J, Patiño D, Miguez JL, Granada E, Moran J, Collazo J. Study of the reaction front thickness in a counter-current fixed-bed combustor of a pelletised biomass. Combustion and Flame 2012;159:1296–302.
[149] Fernandez-Pello a. C, Ray SR, Glassman I. Downward Flame Spread In an Opposed Forced Flow. Combustion Science and Technology 1978;19:19–30.
[150] ASTM. Standard Test Method for Measuring the Minimum Oxygen Concentration to Support Candle-Like Combustion of Plastics (Oxygen Index). 2010.
[151] Johnston MC, T'Ien JS, Muff DE, Zhao X, Olson SL, Ferkul P V. Self induced buoyant blow off in upward flame spread on thin solid fuels. Fire Safety Journal 2015;71:279–86.
[152] Zhu G, Gao Y, Chai G, Zhou J, Gao S. Experimental study of the width effects on self-induced buoyant blow off in upward flame spread over thin fabric fuels. Textile Research Journal 2019.
[153] Olson SL, Ferkul P V., Marcum JW. High-speed video analysis of flame oscillations along a PMMA rod after stagnation region blowoff. Proceedings of the Combustion Institute 2019;37:1555–62.
[154] Matsui K, Koyama A, Uehara K. Fluid-Mechanical Effects on the Combustion Rate of Solid Carbon. Combustion and Flame 1975;25:57–66.
[155] Tsuji H, Matsui K. An aerothermochemical analysis of combustion of carbon in the stagnation flow. Combustion and Flame 1976;26:283–97.